Transient growth without inertia

Mihailo R. Jovanović[1,a)] and Satish Kumar[2,b)]
[1]*Department of Electrical and Computer Engineering, University of Minnesota, Minneapolis, Minnesota 55455, USA*
[2]*Department of Chemical Engineering and Materials Science, University of Minnesota, Minneapolis, Minnesota 55455, USA*

(Received 20 September 2009; accepted 5 January 2010; published online 22 February 2010)

We study transient growth in inertialess plane Couette and Poiseuille flows of viscoelastic fluids. For streamwise-constant three-dimensional fluctuations, we demonstrate analytically the existence of initial conditions that lead to quadratic scaling of both the kinetic energy density and the elastic energy with the Weissenberg number, We. This shows that in strongly elastic channel flows of viscoelastic fluids, both velocity and polymer stress fluctuations can exhibit significant transient growth even in the absence of inertia. Our analysis identifies the spatial structure of the initial conditions (i.e., components of the polymer stress tensor at $t=0$) responsible for this large transient growth. Furthermore, we show that the fluctuations in streamwise velocity and the streamwise component of the polymer stress tensor achieve $\mathcal{O}(\mathrm{We})$ and $\mathcal{O}(\mathrm{We}^2)$ growth, respectively, over a time scale $\mathcal{O}(\mathrm{We})$ before eventual asymptotic decay. We also demonstrate that the large transient responses originate from the stretching of polymer stress fluctuations by a background shear and draw parallels between streamwise-constant inertial flows of Newtonian fluids and streamwise-constant creeping flows of viscoelastic fluids. One of the main messages of this paper is that at the level of velocity fluctuation dynamics, polymer stretching and the Weissenberg number in elasticity-dominated flows of viscoelastic fluids effectively assume the role of vortex tilting and the Reynolds number in inertia-dominated flows of Newtonian fluids. © *2010 American Institute of Physics*. [doi:10.1063/1.3299324]

I. INTRODUCTION

Newtonian fluids, such as air and water, transition to turbulence under the influence of inertia. For low Reynolds numbers (Re), the behavior of Newtonian fluids is dominated by viscous dissipation. As Re increases, the influence of inertia becomes more important and, at large enough Re, flows of these fluids become turbulent. In contrast to Newtonian fluids, viscoelastic fluids may become turbulent (i.e., enter a time-dependent disordered flow state) even at low Re due to additional dynamics associated with the polymeric contribution to the stress tensor.[1–6] Transition to turbulence in viscoelastic fluids is not only of fundamental scientific importance, but is also relevant to practical applications. Examples include the design and control of polymer processing operations and the development of strategies to efficiently mix fluids in microfluidic devices.[7–10]

By now it is well understood that standard linear stability analysis is misleading when it comes to predicting the early stages of transition in wall-bounded shear flows of Newtonian fluids.[11–13] The non-normal nature of the dynamical generator in the linear stability problem allows for initial conditions that grow considerably on finite time intervals before decaying asymptotically due to viscosity.[14] This large growth of initially small perturbations to the linearized equations could put the flow into a regime where nonlinear interactions are no longer negligible. Furthermore, stochastic disturbances to the linearized Navier–Stokes (NS) equations can be significantly amplified, indicating that these equations have high receptivity (i.e., they are exceedingly sensitive to external disturbances) and small robustness margins (i.e., they are exceedingly sensitive to small changes in the underlying model).[15–19] Thus, background disturbances and imperfections in the laboratory environment represent particular examples of *modeling uncertainty* that may conspire to yield experimental observations which are at odds with results from standard linear stability analysis. Alternative analysis methods, dubbed nonmodal stability theory,[13] identify vortex tilting or lift-up as the primary driving force in early stages of transition in Newtonian fluids. This mechanism leads to the creation of alternating regions of high and low streamwise velocity (i.e., streamwise streaks) that are ubiquitous in both experimental[20] and numerical[21–23] studies of transition in wall-bounded shear flows. In contrast, standard linear stability analysis identifies Tollmien–Schlichting (TS) waves as the primary mechanism leading to transition. Yet, the TS waves are only observed in carefully controlled laboratory experiments with very little background noise.[24]

For wall-bounded shear flows of viscoelastic fluids, the dynamical generator in the linear stability problem is also non-normal. This has led a number of researchers to apply the tools of nonmodal stability theory in order to better understand transition in these flows. These analyses have primarily used the Oldroyd-B constitutive equation, the simplest model for a dilute solution of polymer molecules.[8] Both

a)URL: http://umn.edu/home/mihailo/. Electronic mail: mihailo@umn.edu.
b)URL: http://www.cems.umn.edu/research/kumar/. Electronic mail: kumar@cems.umn.edu.

analytical and numerical studies of transient growth phenomena in plane Couette and Poiseuille flows of viscoelastic fluids have been carried out,[25–29] and these show that initial conditions exist which can grow significantly at short times before decaying at long times. The transient growth can occur when fluid inertia is much weaker than fluid elasticity, and even when inertia is completely absent. Except for Ref. 29, the disturbances considered are two dimensional (2D) and in the plane of the base flow. In Ref. 29, three-dimensional (3D) disturbances are studied using the upper convected Maxwell model (a special case of the Oldroyd-B model), but these involve perturbations only to the stresses and not to the velocity field. We note that for plane Couette flow, standard linear stability analysis indicates that the flows of both Newtonian and Oldroyd-B fluids are stable.[30–34] For plane Poiseuille flows, instability is predicted to occur in both Newtonian and Oldroyd-B fluids only above a critical Reynolds number.[35–37]

Experimental observations to date of "elastic turbulence" have been made in curvilinear shear flows rather than in parallel shear flows.[1–5] 3D direct numerical simulations of elasticity-induced transition in such flows under conditions where fluid inertia is present have also been conducted.[38,39] It thus remains an open question whether elastic turbulence can occur in parallel shear flows, and whether elastic turbulence can be sustained when fluid inertia is completely absent. While these issues are beyond the scope of the present study, we lay some groundwork here by considering transient growth of velocity and polymer stress fluctuations in inertialess flows through straight channels. These results could ultimately be used in direct numerical simulations to follow the formation and evolution of coherent structures, similar to what has been done for high-Reynolds-number flows of viscoelastic fluids.[40]

In a recent effort, the present authors investigated nonmodal amplification of exogenous disturbances in plane Couette and Poiseuille flows of Oldroyd-B fluids[41,42] with arbitrary but nonzero Re. The disturbances are 3D in nature, varying harmonically in the streamwise and spanwise directions and stochastically in the wall-normal direction and in time. The results show that the most amplified perturbations are nearly streamwise constant and have an $\mathcal{O}(1)$ spanwise wave number, i.e., they are inherently 3D. Amplification can occur in flows with low (but nonvanishing) Re provided that the level of fluid elasticity is sufficiently strong. The underlying mechanism involves polymer stretching, which transfers energy between polymer stress and velocity fluctuations.[42] These results demonstrate the importance of streamwise streaks even in strongly elastic wall-bounded shear flows of polymer solutions. We note that the early stages of amplification of streaky flow patterns are related to the large receptivity of the linearized governing equations.

The block diagram in Fig. 1(a) provides a systems-level view of the problem considered in Refs. 41 and 42. In these studies, the initial conditions in both velocity and polymer stress fluctuations were set to zero, and the kinetic energy density of flows driven by a spatiotemporal stochastic body forcing **d** was examined. Although this analysis revealed several important aspects of the linearized dynamics of

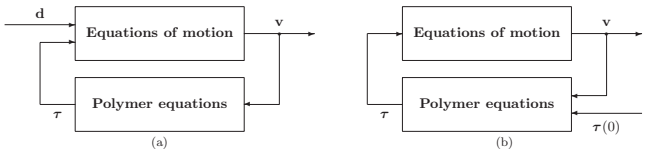

FIG. 1. The block diagram of a flow of a polymeric fluid subject to (a) external body forcing **d** and zero initial conditions in velocity and polymer stress fluctuations and (b) initial conditions in polymer stress fluctuations $\boldsymbol{\tau}(0)$. Note that in general, there may also be initial conditions in velocity fluctuations. However, for creeping flows there is a static-in-time relationship between velocity and polymer stress fluctuations, so only initial conditions for the latter need to be considered.

Oldroyd-B fluids, it leaves open the question of how the linearized system responds to initial conditions. This information is needed in order to completely capture the dynamics of flow fluctuations.[13] In Newtonian fluids, responses to initial conditions and exogenous disturbances reveal similar trends: large transient growth/receptivity, unfavorable scaling with the Reynolds number, and omnipresence of streamwise streaks. However, we show in this paper that for viscoelastic fluids, the presence of initial conditions in polymer stress fluctuations uncovers essential features of the linearized dynamics that were not observed in viscoelastic fluids subject *only* to stochastic body forces. In particular, we demonstrate that both velocity and polymer stress fluctuations in viscoelastic fluids can experience significant transient growth even in the absence of inertia.

We analyze in this work transient growth in plane Couette and Poiseuille flows of viscoelastic fluids. In our analysis we set the Reynolds number to zero, which yields a static-in-time relationship between velocity and polymer stress fields (i.e., inertialess or creeping flow of a polymeric fluid). The motivation for considering creeping flow comes from the observation that polymeric fluids can become turbulent even at very small Re.[1,2] The dynamics of the polymer stress tensor are represented using the Oldroyd-B constitutive equation. In addition to being one of the simplest constitutive models available for polymeric fluids, it has been widely used to interpret experimental observations in viscoelastic fluid flows with constant shear viscosity.[7] Although velocity and polymer stress fluctuations are fully 3D in general, we focus here on the case where the fluctuations are 3D but streamwise constant (i.e., the streamwise wave number k_x is set to zero); our prior work on stochastically driven flows shows that such perturbations are most amplified by the linearized dynamics. Additionally, considerably more analytical progress can be made for this case compared with the case of 2D (streamwise-varying but spanwise-constant) fluctuations. In particular, several explicit scaling relationships are developed and numerically stable results are obtained even at large Weissenberg number, We, which is the ratio of the fluid relaxation time to the characteristic flow time. We note that none of numerical issues encountered in transient growth studies of 2D problems at large We (Ref. 27) are observed here. Furthermore, it should be noted that except for Ref. 29, prior work on transient growth in viscoelastic fluids was restricted to 2D disturbances, while Ref. 29 considers the

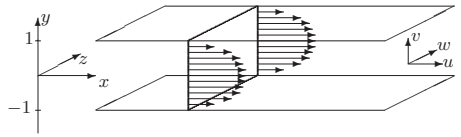

FIG. 2. Schematic of 3D channel flow considered in this work.

special case of 3D polymer stress (but not velocity) fluctuations around a base state for an upper convected Maxwell fluid.

For streamwise-constant 3D fluctuations, we show that both velocity and polymer stress fluctuations can exhibit significant transient growth even in inertialess flows. In particular, we analytically establish that the fluctuations in streamwise velocity and the streamwise component of the polymer stress tensor achieve $\mathcal{O}(\mathrm{We})$ and $\mathcal{O}(\mathrm{We}^2)$ growth, respectively, over a time scale $\mathcal{O}(\mathrm{We})$ before eventual asymptotic decay. Furthermore, we identify the stretching of polymer stress fluctuations by a background shear as the culprit behind this large transient growth and determine the spatial structure of the "worst-case" initial conditions in the polymer stress tensor. Contrary to Ref. 29, these initial conditions *induce* nonzero velocity fluctuations whose value is determined by the equation of motion for creeping flows of an Oldroyd-B fluid.

Our presentation is organized as follows. In Sec. II we describe the governing equations and introduce the streamwise-constant linearized model. Transient responses of velocity and polymer stress fluctuations are considered in Secs. III and IV, respectively. Concluding remarks are offered in Sec. V, and the mathematical developments are relegated to Appendices A–D.

II. PROBLEM SETUP

A. Governing equations and base state

We consider an incompressible flow of a polymeric fluid in a straight 3D channel (Fig. 2). The fluid density is given by ρ, λ is the polymer relaxation time, and η_s, η_p are the solvent and polymeric contributions to the shear viscosity, respectively. By scaling length with the channel half-height L, velocity with the largest base velocity U_o, time with λ, pressure with $(\eta_s+\eta_p)U_o/L$, and polymer stresses with $\eta_p U_o/L$, the equations of motion, continuity, and the polymeric contribution to the stress tensor can be written as

$$\mathrm{Re}\,\dot{\mathbf{V}} = \mathrm{We}[\beta\Delta\mathbf{V} + (1-\beta)\,\nabla\cdot\mathbf{T} - \nabla P - \mathrm{Re}\,\mathbf{V}\cdot\nabla\mathbf{V}], \tag{1a}$$

$$0 = \nabla\cdot\mathbf{V}, \tag{1b}$$

$$\dot{\mathbf{T}} = \mathrm{We}[\mathbf{T}\cdot\nabla\mathbf{V} + (\mathbf{T}\cdot\nabla\mathbf{V})^T - \mathbf{V}\cdot\nabla\mathbf{T}] + \nabla\mathbf{V} + (\nabla\mathbf{V})^T - \mathbf{T}. \tag{1c}$$

Here, a dot identifies a partial derivative with respect to time t, $\mathbf{V}$ is the velocity vector, P is the pressure, $\mathbf{T}$ is the polymer stress tensor, ∇ is the gradient, and $\Delta=\nabla\cdot\nabla$ is the Laplacian. Equation (1) contains three parameters: the Reynolds number, $\mathrm{Re}=\rho U_o L/(\eta_s+\eta_p)$, characterizes the ratio of inertial to viscous forces; the Weissenberg number, $\mathrm{We}=\lambda U_o/L$, captures the product of the polymer relaxation time λ and the typical velocity gradient U_o/L; and the viscosity ratio, $\beta=\eta_s/(\eta_s+\eta_p)$, quantifies the contribution of the solvent to the total viscosity. The constitutive equation [Eq. (1c)] is given for an Oldroyd-B fluid. This equation describes history-dependent elastic deformation and is obtained from kinetic theory by representing each polymer molecule by an infinitely extensible Hookean spring connecting two spherical beads.[8,43]

In shear-driven (Couette) and pressure-driven (Poiseuille) channel flows, Eq. (1) exhibits the steady-state solutions for base velocity $\bar{\mathbf{v}}$ and base polymer stress $\bar{\boldsymbol{\tau}}$,

$$\bar{\mathbf{v}} = \begin{bmatrix} U(y) \\ 0 \\ 0 \end{bmatrix}, \quad \bar{\boldsymbol{\tau}} = \begin{bmatrix} 2\,\mathrm{We}(U'(y))^2 & U'(y) & 0 \\ U'(y) & 0 & 0 \\ 0 & 0 & 0 \end{bmatrix},$$

where y denotes the wall-normal coordinate, $U(y)=y$ in Couette flow, $U(y)=1-y^2$ in Poiseuille flow, and $U'(y)=\mathrm{d}U(y)/\mathrm{d}y$.

In the limit of vanishing inertial forces, i.e., for $\mathrm{Re}=0$, one obtains a creeping flow of an Oldroyd-B fluid for which Eq. (1a) simplifies to the following static-in-time equation:

$$0 = \beta\Delta\mathbf{V} + (1-\beta)\,\nabla\cdot\mathbf{T} - \nabla P. \tag{2}$$

Clearly, for $\beta=1$ Eq. (2) decouples from Eq. (1c) and creeping flow of a Newtonian fluid is recovered.

B. Streamwise-constant linearized model

We confine our study to streamwise-constant 3D fluctuations in creeping flows of an Oldroyd-B fluid. This signifies that the dynamics evolve in the (y,z)-plane, and that the flow fluctuations in all three spatial directions are considered; for example, $\mathbf{v}=\mathbf{v}(y,z,t)=[u\ \ v\ \ w]^T$, where u, v, and w, respectively, denote the streamwise, wall-normal, and spanwise velocity fluctuations. This particular model lends itself to an explicit characterization of the transient growth dependence on the Weissenberg number, as we will show below. We will utilize this explicit We scaling to draw parallels between streamwise-constant inertial flows of Newtonian fluids and creeping flows of Oldroyd-B fluids.

The linearized dynamics can be obtained by decomposing each field in Eqs. (2), (1b), and (1c) into the sum of base and fluctuating parts (e.g., $\mathbf{T}=\bar{\boldsymbol{\tau}}+\boldsymbol{\tau}$), and by neglecting quadratic terms in flow fluctuations in Eq. (1c) (see Appendix A). For streamwise-constant flows, the (y,z)-plane streamfunction ψ can be introduced to rewrite v and w as $\{v=\partial_z\psi, w=-\partial_y\psi\}$, which implies that velocity fluctuations automatically satisfy the continuity equation. Furthermore, the pressure can be eliminated from Eq. (2) to express ψ and u in terms of the polymer stress fluctuation tensor $\boldsymbol{\tau}$. For purely harmonic fluctuations in the z-direction, application of this procedure yields

$$\beta\Delta^2\psi = -(1-\beta)(ik_z\partial_y\tau_{22} - (\partial_{yy}+k_z^2)\tau_{23} - ik_z\partial_y\tau_{33}),$$

$$\beta\Delta u = -(1-\beta)(\partial_y\tau_{12} + ik_z\tau_{13}),$$

where the same notation is used to represent the field [e.g., $\psi(y,z,t)$] and its spanwise Fourier transform [e.g., $\psi(y,k_z,t)$]; the difference between the two should be clear from the context. Here, τ_{ij} with $i,j=\{1,2,3\}$ denotes the ijth component of the polymer stress fluctuation tensor $\boldsymbol{\tau}$,

$$\boldsymbol{\tau} = \begin{bmatrix} \tau_{11} & \tau_{12} & \tau_{13} \\ \tau_{12} & \tau_{22} & \tau_{23} \\ \tau_{13} & \tau_{23} & \tau_{33} \end{bmatrix},$$

k_z is the spanwise wave number, i is the imaginary unit, $\Delta=\partial_{yy}-k_z^2$ with homogeneous Dirichlet boundary conditions, and $\Delta^2=\partial_{yyyy}-2k_z^2\partial_{yy}+k_z^4$ with homogeneous Cauchy (both Dirichlet and Neumann) boundary conditions. Thus, the streamfunction (and consequently v and w) at each time instant depends only on the current value of $\boldsymbol{\tau}_1=[\tau_{22}\ \ \tau_{23}\ \ \tau_{33}]^T$; similarly, the streamwise velocity u is instantaneously equilibrated with the gradient of $\boldsymbol{\tau}_2=[\tau_{12}\ \ \tau_{13}]^T$. To highlight this dependence, we write

$$\psi = \mathbf{C}_\psi\boldsymbol{\tau}_1, \quad u = \mathbf{C}_u\boldsymbol{\tau}_2, \tag{3}$$

where operators $\mathbf{C}_\psi$ and $\mathbf{C}_u$ are given by

$$\mathbf{C}_\psi = -\frac{1-\beta}{\beta}\Delta^{-2}\begin{bmatrix} ik_z\partial_y & -(\partial_{yy}+k_z^2) & -ik_z\partial_y \end{bmatrix},$$

$$\mathbf{C}_u = -\frac{1-\beta}{\beta}\Delta^{-1}\begin{bmatrix} \partial_y & ik_z \end{bmatrix}. \tag{4}$$

We further rearrange the six independent components of the polymer stress tensor $\boldsymbol{\tau}$ into the vector $[\boldsymbol{\tau}_1^T\ \ \boldsymbol{\tau}_2^T\ \ \tau_3]^T$, $\tau_3=\tau_{11}$, and bring the linearization of Eq. (1c) to the form

$$\dot{\boldsymbol{\tau}}_1 = -\boldsymbol{\tau}_1 + \mathbf{F}_{1\psi}\psi, \tag{5a}$$

$$\dot{\boldsymbol{\tau}}_2 = \mathrm{We}(\mathbf{F}_{21}\boldsymbol{\tau}_1 + \mathbf{F}_{2\psi}\psi) + (-\boldsymbol{\tau}_2 + \mathbf{F}_{2u}u), \tag{5b}$$

$$\dot{\tau}_3 = \mathrm{We}^2\mathbf{F}_{3\psi}\psi + \mathrm{We}(\mathbf{F}_{32}\boldsymbol{\tau}_2 + \mathbf{F}_{3u}u) - \tau_3, \tag{5c}$$

where the $\mathbf{F}$-operators are given by Eq. (A2) in Appendix A. A careful examination of the linearized version of constitutive equation (1c) shows that from a physical point of view, $\mathbf{F}_{1\psi}$ and $\mathbf{F}_{2u}$ produce gradients of velocity fluctuations (i.e., $\nabla\mathbf{v}$), $\mathbf{F}_{2\psi}$ captures both transport and stretching of base polymer stress by velocity fluctuations (i.e., $\mathbf{v}\cdot\nabla\overline{\boldsymbol{\tau}}$ and $\overline{\boldsymbol{\tau}}\cdot\nabla\mathbf{v}$), and $\mathbf{F}_{21}$ and $\mathbf{F}_{32}$ represent stretching of polymer stress fluctuations by base shear (i.e., $\boldsymbol{\tau}\cdot\nabla\overline{\mathbf{v}}$). Furthermore, operators $\mathbf{F}_{3\psi}$ and $\mathbf{F}_{3u}$ in Eq. (5c) quantify transport and stretching of a base polymer stress by velocity fluctuations (i.e., $\mathbf{v}\cdot\nabla\overline{\boldsymbol{\tau}}$ and $\overline{\boldsymbol{\tau}}\cdot\nabla\mathbf{v}$), respectively.

Substitution of Eq. (3) into Eq. (5) suggests a one-way coupling from Eq. (5a) to Eq. (5b) and from Eqs. (5a) and (5b) to Eq. (5c),

$$\dot{\boldsymbol{\tau}}_1 = \mathbf{A}_{11}\boldsymbol{\tau}_1, \tag{6a}$$

$$\dot{\boldsymbol{\tau}}_2 = \mathrm{We}\,\mathbf{A}_{21}\boldsymbol{\tau}_1 + \mathbf{A}_{22}\boldsymbol{\tau}_2, \tag{6b}$$

$$\dot{\tau}_3 = \mathrm{We}^2\mathbf{A}_{31}\boldsymbol{\tau}_1 + \mathrm{We}\,\mathbf{A}_{32}\boldsymbol{\tau}_2 - \tau_3, \tag{6c}$$

where the We-independent operators $\mathbf{A}$ are given by Eq. (A3) in Appendix A. Thus, for streamwise-constant fluctuations, we conclude that (i) the dynamics of $\boldsymbol{\tau}_1$ are not influenced by the other polymer stress fluctuations; (ii) the evolution of $\boldsymbol{\tau}_2$ depends on the evolution of $\boldsymbol{\tau}_1$; and (iii) there is no coupling from $\tau_3=\tau_{11}$ to the other polymer stress components in Eq. (6). In particular, this demonstrates that in streamwise-constant creeping flows of Oldroyd-B fluids, evolution of τ_{11} does not influence evolution of $\boldsymbol{\tau}_1$ and $\boldsymbol{\tau}_2$. Since the velocity fluctuation vector $\mathbf{v}$ only depends on $\boldsymbol{\tau}_1$ and $\boldsymbol{\tau}_2$, it follows that evolution of τ_{11} is inconsequential to the dynamics of u, v, and w.

III. TRANSIENT RESPONSE OF VELOCITY FLUCTUATIONS

One of the main objectives of this paper is to show that velocity fluctuations in viscoelastic fluids can experience significant transient growth even in the absence of inertia. This necessitates study of the temporal evolution of the fluctuations' kinetic energy density. In this section, we examine transient growth of this measure of the size of velocity fluctuations as a function of the Weissenberg number. We establish that the presence of initial conditions in $\boldsymbol{\tau}_1$ leads to $\mathcal{O}(\mathrm{We})$ responses of the streamwise velocity fluctuation. In contrast, the responses from all other initial conditions to all other velocity components are We independent. Since the L_2 norm of velocity fluctuations determines kinetic energy, this shows that initial conditions leading to quadratic scaling of the energy density of the streamwise velocity fluctuation with the Weissenberg number can be configured. Therefore, in strongly elastic flows of Oldroyd-B fluids the streamwise velocity can achieve significant transient growth even in the absence of inertia if the initial configuration of the polymers is such that $\boldsymbol{\tau}_1(0)\neq 0$. We also demonstrate that large transient responses arise from stretching of polymers by background shear and provide a comparison of streamwise-constant inertial flows of Newtonian fluids and creeping flows of Oldroyd-B fluids. In particular, we show that at the level of velocity fluctuation dynamics, polymer stretching and the Weissenberg number in elasticity-dominated flows of viscoelastic fluids effectively assume the role of vortex tilting and the Reynolds number in inertia-dominated flows of Newtonian fluids.

A. Kinetic energy density

At any spanwise wave number k_z and time t, the kinetic energy density of velocity fluctuations is captured by

$$E(k_z,t) = \langle\mathbf{v},\mathbf{v}\rangle = E_u(k_z,t) + E_\psi(k_z,t),$$

where $E_u(k_z,t)=\langle u,u\rangle$ and $E_\psi(k_z,t)=\langle v,v\rangle+\langle w,w\rangle = -\langle\psi,\Delta\psi\rangle$. The angular brackets denote the standard $L_2[-1,1]$ inner product, which induces the $L_2[-1,1]$ norm

$$\|\mathbf{v}\|_2^2 = \langle \mathbf{v},\mathbf{v}\rangle = \int_{-1}^{1} \mathbf{v}^*(y,k_z,t)\mathbf{v}(y,k_z,t)\mathrm{d}y,$$

and the asterisk denotes the complex-conjugate transpose of vector $\mathbf{v}$. In view of the observation that $\mathbf{v}$ does not depend on τ_3, we neglect Eq. (6c) in further analysis in this section, yielding the following evolution model:

$$\begin{bmatrix} \dot{\boldsymbol{\tau}}_1 \\ \dot{\boldsymbol{\tau}}_2 \end{bmatrix} = \begin{bmatrix} \mathbf{A}_{11} & 0 \\ \mathrm{We}\,\mathbf{A}_{21} & \mathbf{A}_{22} \end{bmatrix} \begin{bmatrix} \boldsymbol{\tau}_1 \\ \boldsymbol{\tau}_2 \end{bmatrix}, \tag{7a}$$

$$\begin{bmatrix} u \\ v \\ w \end{bmatrix} = \begin{bmatrix} 0 & \mathbf{C}_u \\ \mathbf{C}_v & 0 \\ \mathbf{C}_w & 0 \end{bmatrix} \begin{bmatrix} \boldsymbol{\tau}_1 \\ \boldsymbol{\tau}_2 \end{bmatrix}. \tag{7b}$$

The $\mathbf{A}$-operators determine the dynamical properties of system (7), and the $\mathbf{C}$-operators specify the static-in-time relations between velocity fluctuation components u, v, and w and polymer stress components $\boldsymbol{\tau}_1$ and $\boldsymbol{\tau}_2$. These operators are We independent and they are given by Eqs. (A3) and (A4) in Appendix A. The system of equations (7) is in a form suitable for the analysis carried out in Sec. III B, where we provide an explicit characterization of the We dependence for the transient growth of the velocity fluctuations.

B. Transient growth of kinetic energy density

By making use of basic results from linear systems theory, the lower block-triangular structure of the operator on the right-hand side of Eq. (7a) can be exploited to formally determine the temporal evolution of $\boldsymbol{\tau}_1$ and $\boldsymbol{\tau}_2$,

$$\begin{bmatrix} \boldsymbol{\tau}_1(t) \\ \boldsymbol{\tau}_2(t) \end{bmatrix} = \begin{bmatrix} \mathbf{S}_{11}(t) & 0 \\ \mathrm{We}\,\mathbf{S}_{21}(t) & \mathbf{S}_{22}(t) \end{bmatrix} \begin{bmatrix} \boldsymbol{\tau}_1(0) \\ \boldsymbol{\tau}_2(0) \end{bmatrix}. \tag{8}$$

Here, $\boldsymbol{\tau}_i(0)$ denotes the initial condition in $\boldsymbol{\tau}_i$, i.e., $\boldsymbol{\tau}_i(0)=\boldsymbol{\tau}_i(y,k_z,t=0)$, $i=1,2$. The operator $\mathbf{S}_{ii}(t)$ represents the solution to the equation[44]

$$\dot{\mathbf{S}}_{ii}(t) = \mathbf{A}_{ii}\mathbf{S}_{ii}(t), \quad \mathbf{S}_{ii}(0) = \mathbf{I},$$

where $\mathbf{I}$ is the identity operator and

$$\mathbf{S}_{21}(t) = \int_0^t \mathbf{S}_{22}(t-\xi)\mathbf{A}_{21}\mathbf{S}_{11}(\xi)\mathrm{d}\xi.$$

For notational convenience the dependence on y, k_z, and β is suppressed in the above expressions. More precisely, at any fixed $(\mathrm{We},\beta,k_z,t)$, the $\mathbf{S}$-symbols in Eq. (8) denote operators that map initial values of $\boldsymbol{\tau}_1$ and $\boldsymbol{\tau}_2$ (as a function of y) to the values of $\boldsymbol{\tau}_1$ and $\boldsymbol{\tau}_2$ (as a function of y) at time t, i.e.,

$$\begin{aligned} \boldsymbol{\tau}_1(y,k_z,t) &= [\mathbf{S}_{11}(k_z,t)\boldsymbol{\tau}_1(\cdot,k_z,0)](y), \\ \boldsymbol{\tau}_2(y,k_z,t) &= \mathrm{We}[\mathbf{S}_{21}(k_z,t)\boldsymbol{\tau}_1(\cdot,k_z,0)](y) \\ &\quad + [\mathbf{S}_{22}(k_z,t)\boldsymbol{\tau}_2(\cdot,k_z,0)](y). \end{aligned} \tag{9}$$

It should be also noted that operators $\mathbf{S}_{ij}$ are parametrized by β and that all of them are We independent. By substituting these expressions for $\boldsymbol{\tau}_1(t)$ and $\boldsymbol{\tau}_2(t)$ into Eq. (7b) we finally arrive at

$$\begin{aligned} u(y,k_z,t) &= \mathrm{We}[\mathbf{C}_u(k_z)\mathbf{S}_{21}(k_z,t)\boldsymbol{\tau}_1(\cdot,k_z,0)](y) \\ &\quad + [\mathbf{C}_u(k_z)\mathbf{S}_{22}(k_z,t)\boldsymbol{\tau}_2(\cdot,k_z,0)](y), \\ v(y,k_z,t) &= [\mathbf{C}_v(k_z)\mathbf{S}_{11}(k_z,t)\boldsymbol{\tau}_1(\cdot,k_z,0)](y), \\ w(y,k_z,t) &= [\mathbf{C}_w(k_z)\mathbf{S}_{11}(k_z,t)\boldsymbol{\tau}_1(\cdot,k_z,0)](y). \end{aligned}$$

Several conclusions can now be drawn about dynamics of velocity fluctuations in streamwise-constant creeping flows of Oldroyd-B fluids without doing any detailed computations. First, the responses of wall-normal and spanwise velocity fluctuations are We independent and they are caused by $\boldsymbol{\tau}_1(0)$. Second, the streamwise velocity depends on both $\boldsymbol{\tau}_1(0)$ and $\boldsymbol{\tau}_2(0)$; the contribution of $\boldsymbol{\tau}_2(0)$ to $u(t)$ is We independent and the contribution of $\boldsymbol{\tau}_1(0)$ to $u(t)$ scales linearly with the Weissenberg number. Third, operator $\mathbf{A}_{21}$ in Eq. (7a) is essential to providing affine dependence of $u(t)$ on We; this operator couples $\boldsymbol{\tau}_1$ to $\boldsymbol{\tau}_2$ and if it was zero the responses of all velocity components would be We independent since We would be gone from Eq. (7).

Since the presence of initial conditions in $\boldsymbol{\tau}_1$ introduces $\mathcal{O}(\mathrm{We})$ responses of the streamwise velocity fluctuation, we next examine the maximal transient growth of $u(t)$ (as a function of k_z, t, and β) arising from $\boldsymbol{\tau}_1(0)$. For any fixed $(\mathrm{We},\beta;k_z,t)$, this quantity is determined by

$$\begin{aligned} G_{u1}(\mathrm{We},\beta;k_z,t) &= \sup_{\boldsymbol{\tau}_1(0)\neq 0,\ \boldsymbol{\tau}_2(0)\equiv 0} \frac{\|u(\cdot,k_z,t)\|_2^2}{\|\boldsymbol{\tau}_1(\cdot,k_z,0)\|_2^2} \\ &= \sup_{\|\boldsymbol{\tau}_1(0)\|_2=1,\ \boldsymbol{\tau}_2(0)\equiv 0} \|u(\cdot,k_z,t)\|_2^2 \\ &= \mathrm{We}^2\sigma_{\max}(\mathbf{C}_u(k_z)\mathbf{S}_{21}(\beta;k_z,t)) \\ &= \mathrm{We}^2\bar{G}_{u1}(\beta;k_z,t), \end{aligned} \tag{10}$$

where $\sigma_{\max}(\cdot)$ denotes the largest singular value of a given operator, and $\bar{G}_{u1}(\beta;k_z,t)=\sigma_{\max}(\mathbf{C}_u(k_z)\mathbf{S}_{21}(\beta;k_z,t))$ is a We-independent function. We will also pay attention to the contribution of different components of $\boldsymbol{\tau}_1(0)$ to the transient growth of $u(t)$. For example, $\bar{G}_{u22}(\beta;k_z,t)$ will denote the maximal transient growth of $u(t)$ arising from the initial condition in τ_{22} (with all other initial conditions being set to zero) at $\mathrm{We}=1$; similar notation will be used to quantify the influence of the other two components of $\boldsymbol{\tau}_1(0)$ on $u(t)$. A comprehensive overview of transient growth analysis and its utility in understanding early stages of transition in wall-bounded shear flows of Newtonian fluids can be found in Refs. 12–14.

C. Computation of the transient growth

A more convenient representation for determination of velocity components can be obtained by applying the (temporal) Laplace transform to Eqs. (5a) and (5b) and by substituting the resulting expressions into Eq. (3). This procedure effectively eliminates polymer stresses from the model and transforms Eq. (7) into a system of equations for ψ and u that are driven by the initial conditions in $\boldsymbol{\tau}_1$ and $\boldsymbol{\tau}_2$.

The Laplace transform of Eq. (5a) yields

$$\boldsymbol{\tau}_1(s) = \frac{1}{s+1}[\boldsymbol{\tau}_1(0) + \mathbf{F}_{1\psi}\psi(s)], \quad s \in \mathbb{C}, \tag{11}$$

where $\boldsymbol{\tau}_1(s)$ denotes the Laplace transform of $\boldsymbol{\tau}_1(t)$, with the initial condition $\boldsymbol{\tau}_1(t=0)=\boldsymbol{\tau}_1(0)$. Substitution of this expression to $\psi=\mathbf{C}_\psi\boldsymbol{\tau}_1$ leads to

$$\psi(s) = \frac{1}{s+1/\beta}\mathbf{C}_\psi\boldsymbol{\tau}_1(0), \tag{12}$$

or equivalently in the time domain

$$\psi(y,k_z,t) = \mathrm{e}^{-t/\beta}[\mathbf{C}_\psi\boldsymbol{\tau}_1(\cdot,k_z,0)](y). \tag{13}$$

In arriving at Eq. (13) we have used the fact that $\mathbf{C}_\psi\mathbf{F}_{1\psi}=-(1-\beta)/\beta$. Similarly, substitution of the Laplace transform of Eq. (5b) to $u=\mathbf{C}_u\boldsymbol{\tau}_2$ yields

$$u(s) = \frac{\mathbf{C}_u}{s+1}\{\boldsymbol{\tau}_2(0) + \mathbf{F}_{2u}u(s) + \mathrm{We}[\mathbf{F}_{21}\boldsymbol{\tau}_1(s) + \mathbf{F}_{2\psi}\psi(s)]\}.$$

Now, by observing that $\mathbf{C}_u\mathbf{F}_{2u}=-(1-\beta)/\beta$ and that, in both Poiseuille and Couette flows, $\mathbf{C}_u\mathbf{F}_{2\psi}=0$, we substitute Eqs. (11) and (12) to the last expression to obtain

$$u(s) = \mathrm{We}[g_{1a}(s)\mathbf{H}_{1a} + g_{1b}(s)\mathbf{H}_{1b}]\boldsymbol{\tau}_1(0) + g_2(s)\mathbf{C}_u\boldsymbol{\tau}_2(0). \tag{14}$$

Here,

$$\begin{aligned}\mathbf{H}_{1a} &= \mathbf{C}_u\mathbf{F}_{21} \\ &= -\frac{1-\beta}{\beta}\Delta^{-1}[U''(y) + U'(y)\partial_y \quad \mathrm{i}k_zU'(y) \quad 0], \\ \mathbf{H}_{1b} &= \mathbf{C}_u\mathbf{F}_{21}\mathbf{F}_{1\psi}\mathbf{C}_\psi \\ &= \frac{(1-\beta)^2}{\beta^2}\mathrm{i}k_z\Delta^{-1}[2U''(y)\partial_y + U'(y)\Delta] \\ &\quad \times\Delta^{-2}[\mathrm{i}k_z\partial_y \quad -(\partial_{yy}+k_z^2) \quad -\mathrm{i}k_z\partial_y],\end{aligned} \tag{15}$$

and

$$g_2(s) = \frac{1}{s+1/\beta}, \quad g_{1a}(s) = \frac{g_2(s)}{s+1}, \quad g_{1b}(s) = g_{1a}(s)g_2(s).$$

We note that transformation of Eqs. (12) and (14) to the time domain gives a system of equations for $\psi(y,k_z,t)$ and $u(y,k_z,t)$ driven by the initial conditions in $\boldsymbol{\tau}_1$ and $\boldsymbol{\tau}_2$ mentioned above.

The inverse Laplace transform can now be used to obtain an explicit expression for the streamwise velocity

$$\begin{aligned}u(y,k_z,t) &= \mathrm{We}\,u_1(y,k_z,t) + u_2(y,k_z,t), \\ u_1(y,k_z,t) &= u_{1a}(y,k_z,t) + u_{1b}(y,k_z,t), \\ u_{1r}(y,k_z,t) &= g_{1r}(t)[\mathbf{H}_{1r}\boldsymbol{\tau}_1(\cdot,k_z,0)](y), \quad r=a,b, \\ u_2(y,k_z,t) &= g_2(t)[\mathbf{C}_u\boldsymbol{\tau}_2(\cdot,k_z,0)](y),\end{aligned} \tag{16}$$

where

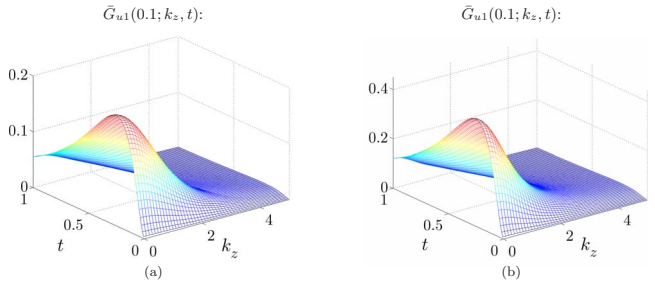

FIG. 3. (Color online) Maximal transient growth of streamwise velocity fluctuations in (a) Couette and (b) Poiseuille flows with $\beta=0.1$ arising from the initial condition in $\boldsymbol{\tau}_1$. All other initial conditions have been set to zero.

$$g_2(t) = \mathrm{e}^{-t/\beta}, \quad g_{1a}(t) = \frac{\beta}{1-\beta}(\mathrm{e}^{-t} - \mathrm{e}^{-t/\beta}),$$

$$g_{1b}(t) = \frac{\beta}{(1-\beta)^2}[\beta(\mathrm{e}^{-t} - \mathrm{e}^{-t/\beta}) - (1-\beta)t\mathrm{e}^{-t/\beta}].$$

Thus, we have managed to provide an explicit characterization of the We dependence for the velocity fluctuations, and to separate the temporal and the spatial parts of their responses. As evident from Eq. (16), the temporal response of streamwise velocity is determined by functions $g_{1r}(t)$ and $g_2(t)$, and the spatial response is characterized by the action of operators $\mathbf{H}_{1r}$ and $\mathbf{C}_u$ on $\boldsymbol{\tau}_1(0)$ and $\boldsymbol{\tau}_2(0)$, respectively.

The above analysis facilitates the derivation of several important conclusions about transient growth of streamwise velocity fluctuations; these follow directly from Eq. (16) and the expressions for operators $(\mathbf{H}_{1r},\mathbf{C}_u)$ and functions $[g_{1r}(t),g_2(t)]$ and do not require any numerical computations. First, as Eq. (16) and the expression for $g_2(t)$ demonstrate, the We-independent contribution to the streamwise velocity, $u_2(y,k_z,t)$, decays monotonically with time. Second, for large values of k_z the response of $u(y,k_z,t)$ is governed by viscous dissipation, i.e., the initial conditions in both $\boldsymbol{\tau}_1$ and $\boldsymbol{\tau}_2$ are "filtered" by the system's dynamics; this is an immediate consequence of the definitions of operators $\mathbf{H}_{1r}$ and $\mathbf{C}_u$ (for additional details, see Appendix B). Third, the We-dependent contribution to the streamwise velocity, $u_1(y,k_z,t)$, exhibits a transient growth in time, as indicated by the formulas for $g_{1a}(t)$ and $g_{1b}(t)$; furthermore, from Eqs. (15) and (16), it follows that at $k_z=0$, the response caused by either $\tau_{23}(0)$ or $\tau_{33}(0)$ disappears (see Appendix B). This observation, in conjunction with the fact that viscous dissipation "filters" responses for large spanwise wave numbers, suggests the presence of peaks at nonzero k_z in the transient growth functions $\bar{G}_{u23}(\beta;k_z,t)$ and $\bar{G}_{u33}(\beta;k_z,t)$. On the other hand, Eq. (15) indicates that the initial conditions in τ_{22} lead to nonzero responses of streamwise velocity even at $k_z=0$ (see Appendix B). Thus, numerical computations are necessary to determine the value of k_z at which $\bar{G}_{u22}(\beta;k_z,t)$ peaks; the computations conducted below suggest that this function achieves its maximum at $k_z=0$.

The function characterizing maximal transient growth of streamwise velocity fluctuations arising from the initial conditions in $\boldsymbol{\tau}_1$ [cf. Eq. (10)] in flows with $\beta=0.1$,

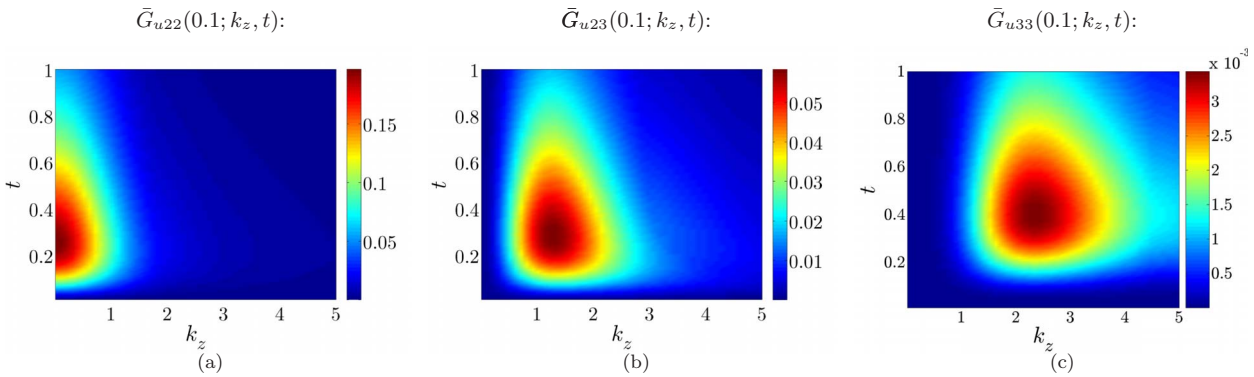

FIG. 4. (Color online) Maximal transient growth of streamwise velocity fluctuations in Couette flow with $\beta=0.1$ arising from the initial condition in (a) τ_{22}, (b) τ_{23}, and (c) τ_{33}. All other initial conditions have been set to zero.

$\bar{G}_{u1}(0.1;k_z,t)$, is shown in Fig. 3; results for other values of β look similar and are not reported here for brevity. The finite-dimensional approximations of the wall-normal operators $\mathbf{H}_{1a}$ and $\mathbf{H}_{1b}$ in the expression for $u_1(y,k_z,t)$ [cf. Eqs. (15) and (16)] are obtained using the pseudospectral method.[45] All computations are performed in MATLAB with 50 Gauss–Lobatto points in the wall-normal direction; additional computations with a much larger number of grid points in y were used to confirm convergence. We observe similar trends in both Couette and Poiseuille flows with peak values of $\bar{G}_{u1}(0.1;k_z,t)$ occurring at $k_z=0$ and $t\approx 0.25$. From the above discussion, it immediately follows that the largest contribution to the transient growth of u comes from the initial conditions in τ_{22}; this is because the maximal transient growth happens at $k_z=0$ and only $\tau_{22}(0)$ contributes to $\bar{G}_{u1}(\beta;k_z=0,t)$. This is further illustrated in Fig. 4, where maximal transient growth of streamwise velocity fluctuations caused by the different components of $\boldsymbol{\tau}_1(0)$ in Couette flow with $\beta=0.1$ is shown. The peak values in Fig. 4(a) are about three times larger than the peak values in Fig. 4(b), and about 60 times larger than the peak values in Fig. 4(c). This suggests that the initial conditions in τ_{22} create the largest transient growth of the streamwise velocity fluctuations, followed by the initial conditions in τ_{23}, followed by the initial conditions in τ_{33}. It is also noteworthy that the peaks of functions $\bar{G}_{u23}(0.1;k_z,t)$ and $\bar{G}_{u33}(0.1;k_z,t)$ occur at nonzero values of k_z; on the other hand, similar to $\bar{G}_{u1}(0.1;k_z,t)$, function $\bar{G}_{u22}(0.1;k_z,t)$ achieves its maximum at $k_z=0$. These computations confirm our *a priori* predictions obtained from the analysis of Eqs. (15) and (16) above.

The functions characterizing the largest transient growth of u caused by the initial conditions in τ_{22}, τ_{23}, and τ_{33}, in Poiseuille flow with $\beta=0.1$, are shown in Fig. 5. We observe similar trends as in Couette flow; $\tau_{22}(0)$ induces the largest transient growth of the streamwise velocity fluctuations, followed by $\tau_{23}(0)$, followed by $\tau_{33}(0)$. Relative to Couette flow, the peak value of function $\bar{G}_{u22}(0.1;k_z,t)$ is larger, and the peak values of $\bar{G}_{u23}(0.1;k_z,t)$ and $\bar{G}_{u33}(0.1;k_z,t)$ are smaller. We also note that $\bar{G}_{u22}(0.1;k_z,t)$ looks very similar in both flows, and that $\bar{G}_{u23}(0.1;k_z,t)$ has a slightly broader k_z-spectrum in Poiseuille flow than in Couette flow; furthermore, the peak of this function has moved to slightly larger value of k_z [peaks in Figs. 4(b) and 5(b), respectively, take place at $k_z\approx 1.29$ and $k_z\approx 1.64$]. The most noticeable difference is observed in responses of u caused by the initial conditions in τ_{33}; in Couette flow, transient growth function $\bar{G}_{u33}(0.1;k_z,t)$ has a single peak at $(t\approx 0.4,\ k_z\approx 2.35)$, whereas in Poiseuille flow, this function has two peaks at $(t\approx 0.4,\ k_z\approx 2.44)$ and $(t\approx 0.4,\ k_z\approx 4.1)$. The spatial distribution of the initial conditions (in different components of

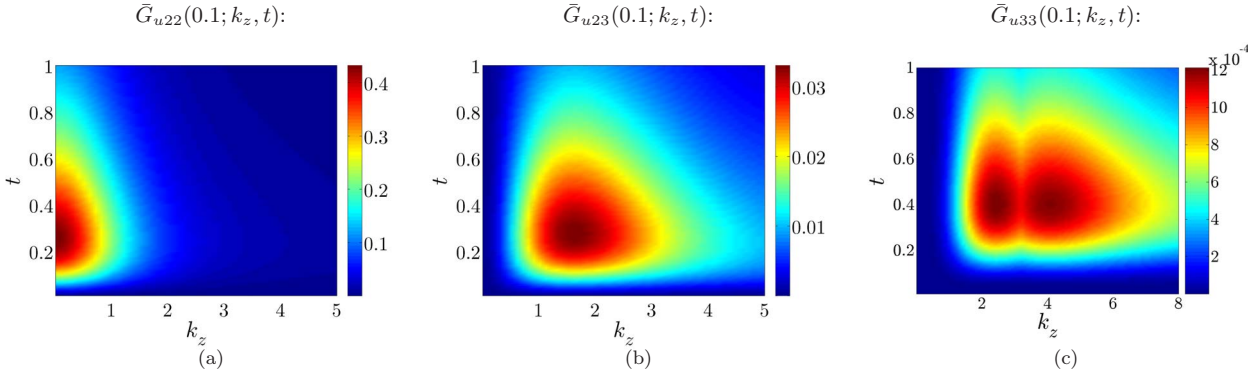

FIG. 5. (Color online) Maximal transient growth of streamwise velocity fluctuations in Poiseuille flow with $\beta=0.1$ arising from the initial condition in (a) τ_{22}, (b) τ_{23}, and (c) τ_{33}. All other initial conditions have been set to zero.

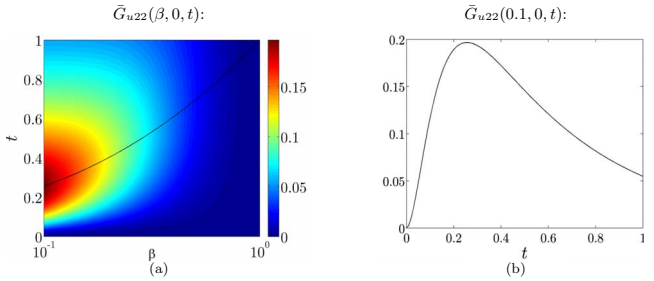

FIG. 6. (Color online) Maximal transient growth of streamwise velocity fluctuations in Couette flow with $k_z=0$ (a) as a function of β and t and (b) as a function of t at $\beta=0.1$. The black line in plot (a) shows times as a function of β, at which maximal transient growth is attained. Apart from $\tau_{22}(0)$, all other initial conditions have been set to zero.

$\boldsymbol{\tau}_1$) leading to the peaks observed in Figs. 4 and 5 is discussed in Sec. III D; the resulting streamwise velocity flow structures are also described in Sec. III D.

Motivated by the observation that the largest transient growth of energy density for streamwise-constant velocity fluctuations takes place at $k_z=0$, we next examine the linearized model with both $k_x=0$ and $k_z=0$. From the analysis of this model in Appendix C it follows that the streamwise velocity $u(y,t)$ can be represented as

$$u(y,t) = \mathrm{We}\, u_{22}(y,t) + \mathrm{e}^{-t/\beta} u(y,0),$$
$$u_{22}(y,t) = -(\mathrm{e}^{-t} - \mathrm{e}^{-t/\beta})[\partial_{yy}^{-1}(U''(y) + U'(y)\partial_y)\tau_{22}(\cdot,0)](y). \quad (17)$$

This indicates that the initial conditions in the streamwise velocity [or, equivalently, in τ_{12}; from Eq. (C1) it follows that $u(y,t)=-(1/\beta-1)[\partial_{yy}^{-1}\partial_y\tau_{12}(\cdot,t)](y)$] create monotonically decaying We-independent responses of $u(y,t)$, with a rate of decay inversely proportional to the viscosity ratio β. On the other hand, even though $\tau_{22}(y,0)\neq 0$ yields zero initial kinetic energy (see Appendix C), the presence of initial conditions in τ_{22} generates streamwise velocity fluctuations, We $u_{22}(y,t)$, which scale linearly with the Weissenberg number and also exhibit temporal transient growth (see Fig. 6 for an illustration). We note that this feature arises solely from viscoelastic nature of the underlying fluid, and that the approach that allows for fluctuations in polymer stresses *but not* in velocities fails to identify it.[29] Figure 6(a) shows the maximal transient growth of u_{22} in Couette flow as a function of β and t. The black line in this plot indicates time instants, as a function of β, at which maximal transient growth is attained, $t=\beta/(1-\beta)\log(1/\beta)$. In Poiseuille flow, the maximal transient growth at $k_z=0$ has the same (t,β)-dependence as in Couette flow; the only difference is that the values shown in Fig. 6 should be multiplied by the ratio of the maximal singular values of the operators in the expression for $u_{22}(y,t)$ in Poiseuille and Couette flows, $2\sigma_{\max}(\partial_{yy}^{-1}(1+y\partial_y))/\sigma_{\max}(\partial_{yy}^{-1}\partial_y)\approx 2.2$. It should be noted that if the time was normalized by the characteristic flow time scale, L/U_o, the transient growth of u would take place over an $\mathcal{O}(\mathrm{We})$ time scale before eventual asymptotic decay.

D. Dominant flow structures

In this section, we discuss the spatial distribution of the initial conditions (in τ_{22}, τ_{23}, and τ_{33}) and the resulting streamwise velocity flow patterns corresponding to the transient growth peaks observed in Figs. 4 and 5. These structures are purely harmonic in the spanwise direction and their wall-normal shapes are determined by the principal singular functions of the operators mapping different components of $\boldsymbol{\tau}_1(\cdot,k_z,0)$ to $u(\cdot,k_z,t)$.[14] The singular value decomposition is performed at the values of k_z and t, where the transient growth functions of Figs. 4 and 5 achieve their respective maxima.

Structures of the initial conditions in τ_{23} and τ_{33} leading to the largest transient growth of u, in Couette flow with $\beta=0.1$, are shown in Figs. 7(b) and 7(c). The peaks of functions $\bar{G}_{23}$ and $\bar{G}_{33}$ [cf. Figs. 4(b) and 4(c)] take place at $(k_z\approx 1.29,\ t\approx 0.29)$ and $(k_z\approx 2.35,\ t\approx 0.4)$, respectively, and these worst case initial conditions are obtained by performing a singular value decomposition of the operators mapping $\tau_{23}(\cdot,1.29,0)$ to $u(\cdot,1.29,0.29)$ and $\tau_{33}(\cdot,2.35,0)$ to $u(\cdot,2.35,0.4)$ at We=1. Similarly, Fig. 7(a) illustrates the $\tau_{22}(0)$ that creates the largest transient growth of u at $k_z=1.29$. Since the underlying model driven by $\tau_{22}(0)$ is not capable of selecting the preferential spanwise length scale, this value of k_z is chosen in order to compare the resulting flow patterns with the ones obtained in a flow subject to the worst case initial condition in τ_{23}. In Couette flow with

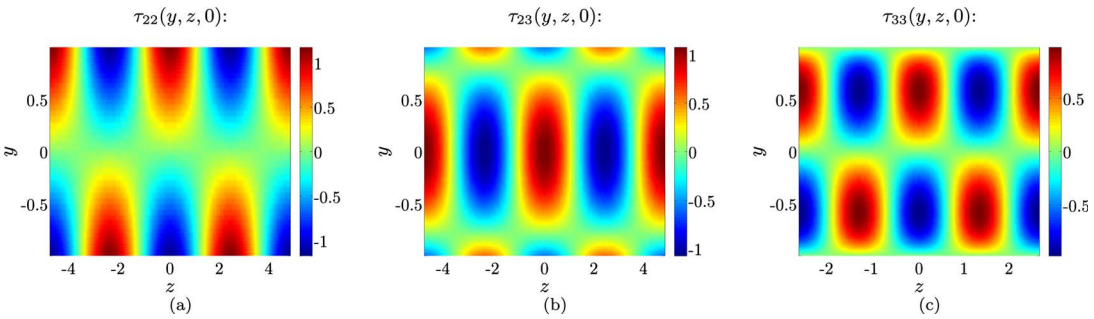

FIG. 7. (Color online) Structures of the components of $\boldsymbol{\tau}_1(0)$ leading to the largest transient growth of streamwise velocity fluctuations in Couette flow with $\beta=0.1$ and (a) $k_z=1.29$, $t=0.23$; (b) $k_z=1.29$, $t=0.29$; and (c) $k_z=2.35$, $t=0.4$.

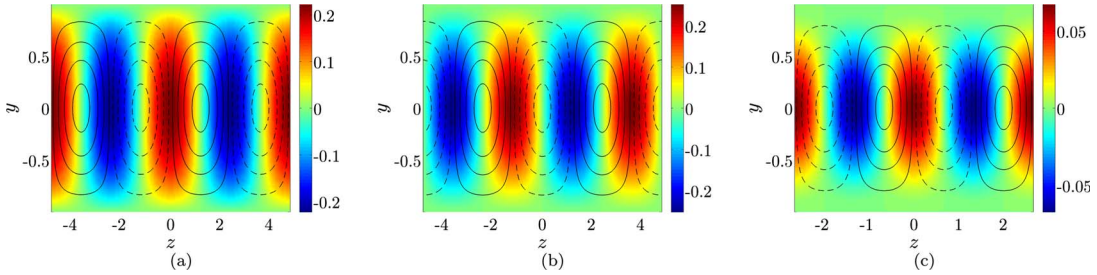

FIG. 8. (Color online) Dominant flow structures in Couette flow subject to the initial conditions shown in Figs. 7(a)–7(c), respectively. The shaded plots represent streamwise velocity and the contour lines represent streamfunction fluctuations.

$\beta=0.1$ and $k_z=1.29$, the transient growth function $\bar{G}_{22}$ achieves its largest value of 0.0560 at $t\approx 0.23$ (in comparison, max $\bar{G}_{23}\approx 0.0586$). The initial conditions shown in Fig. 7 are normalized so that $\|\tau_{ij}(\cdot,k_z,0)\|_2=1$, for each $i,j=2,3$, and they are characterized by alternating regions of high and low polymer stress values. The initial condition in τ_{33} vanishes at the walls, while $\tau_{22}(0)$ and $\tau_{23}(0)$ have nonzero wall values with the largest values of $\tau_{22}(0)$ being at the walls. Furthermore, both $\tau_{22}(0)$ and $\tau_{33}(0)$ are antisymmetric, while $\tau_{23}(0)$ is symmetric with respect to the channel centerline. Dominant flow structures in Couette flow with $\beta=0.1$ subject to the initial conditions of Figs. 7(a)–7(c) are shown in Figs. 8(a)–8(c), respectively. The shaded plots represent streamwise velocity and the contour lines represent streamfunction fluctuations; the solid (dashed) contour lines denote the positive (negative) values of ψ. As in inertial flows of Newtonian fluids,[14] the dominant flow patterns assume the form of streamwise streaks that are symmetric with respect to the channel centerline with pairs of counter-rotating streamwise vortices in between them. Vortices in Fig. 8 occupy the entire channel width; furthermore, they transport low-velocity fluid away from the walls and redistribute it in the spanwise direction.

The spatial distributions of the initial conditions in τ_{23} and τ_{33} leading to the peaks observed in Figs. 5(b) and 5(c) (Poiseuille flow) are illustrated in Fig. 9, and the induced dominant flow patterns are shown in Fig. 10. The worst-case initial condition in τ_{23} [cf. Fig. 9(a)], which is antisymmetric with respect to the channel centerline with nonzero wall values, results in symmetric peaks in u with pairs of counter-rotating vortices in both the upper and the lower halves of the channel [cf. Fig. 10(a)]. The developed structures are reminiscent of the "best energy optima" determined in the transient growth analysis in subcritical Poiseuille flow of Newtonian fluids.[14] We note that the dominant flow patterns obtained in the presence of $\tau_{22}(\cdot,1.64,0)$ have similar spatial profiles (not shown here). In contrast, the two peaks in the transient growth function $\bar{G}_{33}$ [cf. Fig. 5(c)] result in vastly different initial conditions in τ_{33} and corresponding dominant flow structures. The peak at $k_z=2.44$ in Fig. 5(c) is caused by the antisymmetric initial condition [cf. Fig. 9(b)] which yields the antisymmetric response in u with vortices occupying the entire channel width [cf. Fig. 10(b)]. Conversely, the peak at $k_z=4.1$ in Fig. 5(c) comes from symmetric $\tau_{33}(0)$ [cf. Fig. 9(c)] which induces the symmetric response in u with two vortices that fit into the channel width [cf. Fig. 10(c)].

We close this section by computing the worst case initial conditions of τ_{22} and the resulting responses of u in both Couette and Poiseuille flows. As described above, the transient growth function $\bar{G}_{22}$ achieves its peak value at $k_z=0$ and $t=\beta/(1-\beta)\log(1/\beta)$. In Couette flow, the operator mapping $\tau_{22}(\cdot,0)$ into $u_{22}(\cdot,t)$ simplifies to [cf. Eq. (17)]

$$u_{22}(y,t)=-(e^{-t}-e^{-t/\beta})[\partial_{yy}^{-1}\partial_y\tau_{22}(\cdot,0)](y).$$

Singular value decomposition of this operator provides an explicit characterization of the initial condition/response pair $[\tau_{22}(y,0),u_{22}(y,t)]$ corresponding to the largest transient growth

$$\tau_{22}(y,0)=c-\cos[\pi/2(y+1)],$$

$$u_{22}(y,t)=2/\pi(e^{-t}-e^{-t/\beta})\sin[\pi/2(y+1)],$$

where c is an arbitrary constant. The initial conditions in τ_{22} along with the corresponding streamwise velocity fluctua-

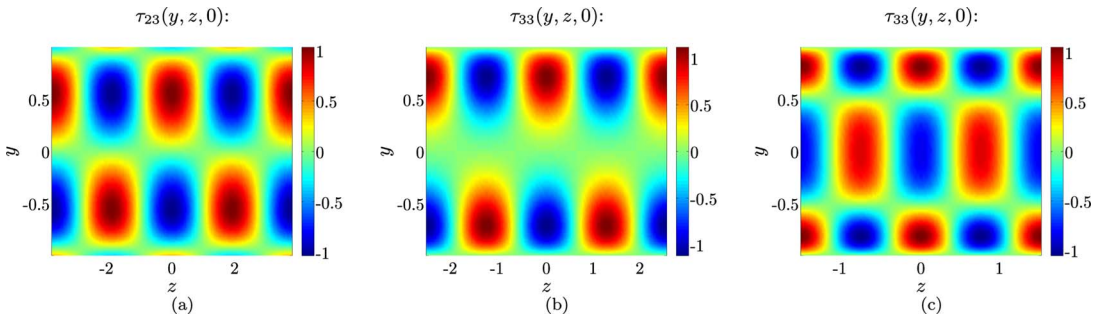

FIG. 9. (Color online) Structures of $\tau_{23}(0)$ and $\tau_{33}(0)$ leading to the largest transient growth of streamwise velocity fluctuations in Poiseuille flow with $\beta=0.1$ and: (a) $k_z=1.64$, $t=0.28$; (b) $k_z=2.44$, $t=0.4$; and (c) $k_z=4.1$, $t=0.4$.

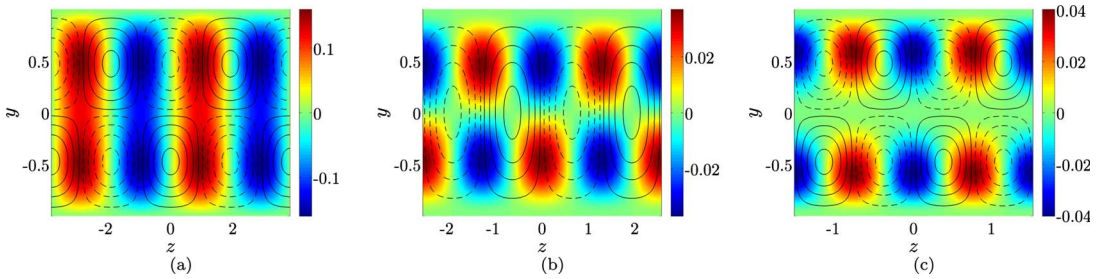

FIG. 10. (Color online) Dominant flow structures in Poiseuille flow subject to the initial conditions shown in Figs. 9(a)–9(c), respectively. The shaded plots represent streamwise velocity and the contour lines represent streamfunction fluctuations.

tions, in both Couette and Poiseuille flows with $\beta=0.1$ and $t=\beta/(1-\beta)\log(1/\beta)\approx 0.25$, are illustrated in Fig. 11. The results in Poiseuille flow are obtained numerically in MATLAB using the numerical scheme described in Ref. 45, and $\tau_{22}(y,0)$ in Couette flow is given for $c=0$.

Finally, we comment on the lack of intrinsic wavelength selection in the Oldroyd-B model driven by $\tau_{22}(0)$. Our analysis is conducted in a channel that is infinitely long in the horizontal directions and the question of spontaneous occurrence and physical realizability of these worst case initial conditions in experiments remains; in particular, flow fluctuations with large horizontal wavelength cannot be realized in the laboratory. Thus, the presence of sidewalls in an experimental channel flow configuration, the level of background disturbances, and the initial distribution of polymer stress components would all impact the length scale selection. Furthermore, we note that experimental and direct numerical simulation results for Newtonian fluids are characterized by the interaction of different modes rather than by a dominance of one particular mode. Thus, the development of the velocity fluctuations in a real viscoelastic flow is anticipated to be much more complicated than the structures shown in this section. Nevertheless, the performed analysis identifies the physical mechanism responsible for large transient growth (see Sec. III E) and it serves as an indication of flow patterns that can be expected to be seen in both experimental and numerical investigations of early stages of transition in viscoelastic fluids. It is also noteworthy that similar

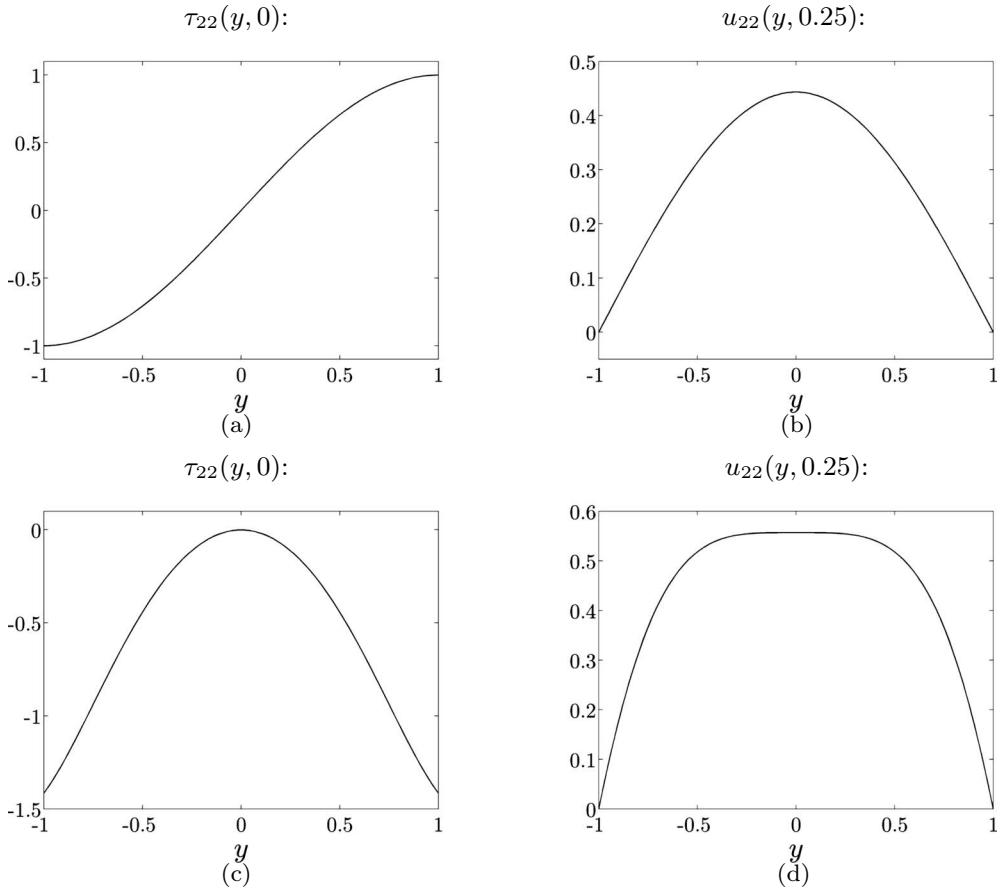

FIG. 11. Structures of $\tau_{22}(y,0)$ and $u_{22}(y,0.25)$ corresponding to the largest transient growth of streamwise velocity fluctuations in Couette (first row) and Poiseuille (second row) flows with $k_z=0$, $\beta=0.1$, and $t=\beta/(1-\beta)\log(1/\beta)\approx 0.25$.

lack of an intrinsic length scale was recently observed in the analysis of the dynamics of a stochastically forced Lamb–Oseen vortex;[46] the authors eloquently explained the utility of nonmodal stability theory in understanding the problem at hand in spite of the issues with identification of the prevalent wavelength.

E. Comparison to inertial flows of Newtonian fluids

We next provide comparison of the above results to those for inertial flows of Newtonian fluids. By scaling length with the channel half height L, velocity with the largest base velocity U_o, and time with the diffusive time $\rho L^2/\eta_s$, the linearized evolution model for streamwise-constant fluctuations assumes the following form:

$$\begin{bmatrix} \dot{\phi}_1 \\ \dot{\phi}_2 \end{bmatrix} = \begin{bmatrix} \overline{\mathbf{A}}_{11} & 0 \\ \mathrm{Re}\,\overline{\mathbf{A}}_{21} & \overline{\mathbf{A}}_{22} \end{bmatrix} \begin{bmatrix} \phi_1 \\ \phi_2 \end{bmatrix}, \tag{18a}$$

$$\begin{bmatrix} u \\ v \\ w \end{bmatrix} = \begin{bmatrix} 0 & \overline{\mathbf{C}}_u \\ \overline{\mathbf{C}}_v & 0 \\ \overline{\mathbf{C}}_w & 0 \end{bmatrix} \begin{bmatrix} \phi_1 \\ \phi_2 \end{bmatrix}. \tag{18b}$$

This model is obtained by eliminating pressure from the linearized NS equations and by expressing flow fluctuations in terms of the (y,z)-plane streamfunction $\phi_1=\psi$ (cf. Sec. II B) and the streamwise velocity $\phi_2=u$. Here, $\mathrm{Re}=\rho U_o L/\eta_s$ denotes the Reynolds number, and operators $\overline{\mathbf{A}}$ and $\overline{\mathbf{C}}$ are given by

$$\overline{\mathbf{A}}_{11}=\Delta^{-1}\Delta^2, \quad \overline{\mathbf{A}}_{22}=\Delta, \quad \overline{\mathbf{A}}_{21}=-\mathrm{i}k_z U'(y),$$

$$\overline{\mathbf{C}}_u=\mathbf{I}, \quad \overline{\mathbf{C}}_v=\mathrm{i}k_z, \quad \overline{\mathbf{C}}_w=-\partial_y,$$

with Dirichlet boundary conditions on Δ and Cauchy boundary conditions on Δ^2. Note that $\overline{\mathbf{A}}_{11}$, $\overline{\mathbf{A}}_{22}$, and $\overline{\mathbf{A}}_{21}$, respectively, denote the Orr–Sommerfeld, Squire, and coupling operators in the streamwise-constant linearized NS equations with $\mathrm{Re}=1$.[12]

Direct comparison of Eqs. (7) and (18) reveals a striking structural similarity between streamwise-constant creeping flows of Oldroyd-B fluids and inertial flows of Newtonian fluids. In particular, these two equations can be represented graphically by the corresponding block diagrams in Figs. 12(a) and 12(b), respectively. The enabling mechanism for transient growth in Newtonian fluids is vortex tilting, which is embedded in operator $\overline{\mathbf{A}}_{21}=-\mathrm{i}k_z U'(y)$. In the absence of vortex tilting, the responses of all velocity components are Re independent and the dynamical properties of streamwise-constant flows of Newtonian fluids are governed by viscous dissipation. On the other hand, the key physical mechanism for transient growth in creeping flows of Oldroyd-B fluids is polymer stretching, which is embedded in operator $\mathbf{A}_{21}=\mathbf{F}_{21}+\mathbf{F}_{2\psi}\mathbf{C}_\psi$ (cf. Sec. II B and Appendix A). We also

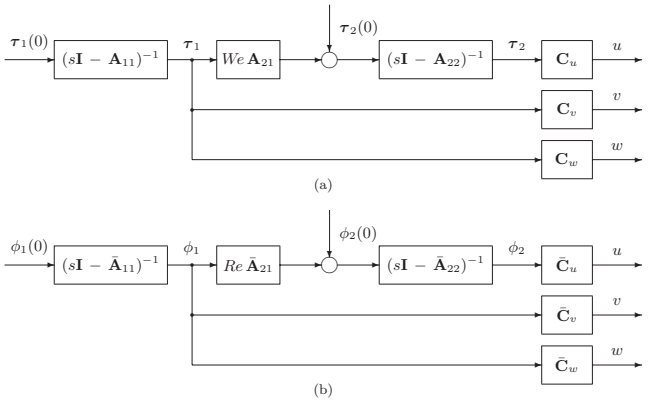

FIG. 12. The block diagrams of (a) streamwise-constant creeping flows of Oldroyd-B fluids, cf. Eq. (7), and (b) streamwise-constant inertial flows of Newtonian fluids, cf. Eq. (18). In Newtonian fluids transient growth comes from vortex tilting, i.e., operator $\overline{\mathbf{A}}_{21}$, and in viscoelastic fluids it comes from polymer stretching, i.e., operator $\mathbf{A}_{21}$. Note that the Weissenberg number in creeping flows of viscoelastic fluids assumes the role of the Reynolds number in inertial flows of Newtonian fluids.

observe that the Weissenberg number in viscoelastic fluids has a role similar to that of the Reynolds number in Newtonian fluids.

The above comparison suggests remarkable similarities between streamwise-constant creeping flows of Oldroyd-B fluids and streamwise-constant inertial flows of Newtonian fluids. All these similarities are exhibited at the level of velocity fluctuation dynamics. Namely, as far as kinetic energy density is concerned, it is conceptually useful to think of creeping flows of Oldroyd-B fluids in terms of inertial flows of Newtonian fluids. This analogy is made keeping in mind that polymer stretching and the Weissenberg number in elasticity-dominated flows of viscoelastic fluids effectively take the role of vortex tilting and the Reynolds number in inertia-dominated flows of Newtonian fluids.

Despite these similarities there are several important fundamental differences between creeping flows of Oldroyd-B fluids and inertial flows of Newtonian fluids. First, as the results of Sec. III C demonstrate, $\mathcal{O}(\mathrm{We})$ responses of streamwise velocity fluctuations can be obtained in viscoelastic fluids even at $k_x=k_z=0$. These responses are caused by the initial conditions in τ_{22} and they are without parallel in Newtonian fluids. Namely, the linearized NS equations with $k_x=k_z=0$ simplify to two decoupled diffusion equations for the streamwise and spanwise velocity fluctuations,

$$\dot{u}=\partial_{yy}u, \quad \dot{w}=\partial_{yy}w,$$

which shows dominance of viscous dissipation and monotonic temporal decay of both u and w. On the other hand, in the viscoelastic case w decays monotonically with time, $w(y,t)=\mathrm{e}^{-t/\beta}w(y,0)$, but the dynamics of u are governed by (cf. Appendix C)

$$\left.\begin{aligned}\dot{\tau}_{22} &= -\tau_{22}\\ \dot{\tau}_{12} &= -\tau_{12} + \partial_y u + \mathrm{We}\, U'(y)\tau_{22}\\ u &= -(1/\beta - 1)\partial_{yy}^{-1}\partial_y \tau_{12}\end{aligned}\right\} \Leftrightarrow \left\{\begin{aligned}\dot{\tau}_{22} &= -\tau_{22},\\ \dot{u} &= -(1/\beta)u - \mathrm{We}(1/\beta - 1)\partial_{yy}^{-1}[U''(y) + U'(y)\partial_y]\tau_{22}.\end{aligned}\right.$$

We notice that the monotonically decaying response of τ_{22}, $\tau_{22}(y,t)=e^{-t}\tau_{22}(y,0)$, couples into the equation for the streamwise velocity through a term which is proportional to We. This coupling, which physically comes from the stretching of τ_{22} by a background shear [i.e., operator $\mathbf{F}_{21}$ in Eq. (5b)], is the culprit behind the transient growth in time and the linear scaling of $u(y,t)$ with the Weissenberg number observed earlier. Second, while kinetic energy density represents a relevant measure of the size of velocity fluctuations, this quantity is not suitable for capturing evolution of polymer stress fluctuations. The transient growth of stresses also needs to be assessed as it could trigger nonlinearities and cause secondary instability to streamwise-varying flow fluctuations. In Sec. IV, we consider the response of polymer stress fluctuations and examine the transient growth of the elastic energy stored in polymers.

IV. TRANSIENT RESPONSE OF POLYMER STRESS FLUCTUATIONS

In Sec. III, we have demonstrated that streamwise-constant velocity fluctuations in creeping channel flows of Oldroyd-B fluids can experience a significant transient growth. We next examine the transient response of polymer stress fluctuations and show that the nonzero initial contribution of τ_{22} to the elastic energy leads to $\mathcal{O}(\mathrm{We}^2)$ responses of the elastic energy. This We^2-scaling comes from the stretching of polymer stress fluctuations by a background shear and it is accompanied by a transient growth in time of τ_{11}. We provide an explicit expression for the temporal transient growth and identify time instants at which elastic energy stored in polymers achieves its largest value in both Couette and Poiseuille flows. Contrary to the results of Sec. III, the transient response of polymer stress fluctuations does not decay for large values of k_z, which is a consequence of the lack of a diffusion in the constitutive equations. Our numerical computations indicate that the addition of a small amount of stress diffusion does not bring any significant changes into the response of velocity fluctuations; conversely, this addition introduces a high-wavenumber roll-off into the response of polymer stress fluctuations.

A. Elastic energy of polymer stress fluctuations

The elastic energy of polymer stress fluctuations in channel flows is captured by $\Pi(t)=\Sigma_{i=1}^{3}\Pi_{ii}(t)$, where $\Pi_{ii}(t)$ denotes the contribution of τ_{ii} to $\Pi(t)$,

$$\Pi_{ii}(t) = \frac{1}{2}\int_{-1}^{1}\int_{-\infty}^{\infty}\int_{-\infty}^{\infty}\tau_{ii}(x,y,z,t)\mathrm{d}x\mathrm{d}z\mathrm{d}y.$$

It should be noted that the trace of the polymeric contribution to the stress tensor is directly proportional to the mean-square end-to-end distance of the Hookean dumbbell on which the Oldroyd-B model is based (see Sec. 13.2 of Ref. 43); $\Pi(t)$ thus captures the deviation of the mean-square end-to-end distance from its base value.

Since the Fourier transform of each τ_{ii} is given by

$$\tau_{ii}(k_x,y,k_z,t) = \int_{-\infty}^{\infty}\int_{-\infty}^{\infty}\tau_{ii}(x,y,z,t)e^{-\mathrm{i}(k_x x + k_z z)}\mathrm{d}x\mathrm{d}z,$$

it follows that $\Pi_{ii}(t)$ can equivalently be determined from

$$\Pi_{ii}(t) = \frac{1}{2}\int_{-1}^{1}\tau_{ii}(y,t)\mathrm{d}y,$$

where $\tau_{ii}(y,t)$ denotes the Fourier transform of τ_{ii} evaluated at $k_x=k_z=0$, i.e., $\tau_{ii}(y,t)=\tau_{ii}(k_x=0,y,k_z=0,t)$. Therefore, the transient growth of elastic energy stored in infinitesimal polymer stress fluctuations is governed by the linearized evolution model at $k_x=k_z=0$.

From Eq. (C2a) in Appendix C we conclude that

$$\dot{\tau}_{ii}(y,t) = -\tau_{ii}(y,t), \quad i=2,3,$$

which implies that the contributions of both τ_{22} and τ_{33} to the elastic energy decay monotonically with time, i.e.,

$$\Pi_{ii}(t) = e^{-t}\Pi_{ii}(0), \quad i=2,3.$$

On the other hand, the temporal evolution of Π_{11} can be ascertained by analyzing the following system of equations [see Eq. (6) and Appendix C]:

$$\dot{\tau}_{22} = -\tau_{22}, \tag{19a}$$

$$\dot{\tau}_{12} = -\tau_{12} + \partial_y u + \mathrm{We}\, U'(y)\tau_{22}, \tag{19b}$$

$$\dot{\tau}_{11} = -\tau_{11} + 2\,\mathrm{We}\, U'(y)(\partial_y u + \tau_{12}). \tag{19c}$$

In Couette flow, Eq. (19) simplifies to

$$\dot{\tau}_{22} = -\tau_{22},$$

$$\dot{\tau}_{12} = -\tau_{12} + \partial_y u + \mathrm{We}\,\tau_{22},$$

$$\dot{\tau}_{11} = -\tau_{11} + 2\,\mathrm{We}(\partial_y u + \tau_{12}),$$

and the wall-normal integration of these equations, in conjunction with Dirichlet boundary conditions on u, yields

$$\dot{\Pi}_{22}(t) = -\Pi_{22}(t),$$

$$\dot{\Pi}_{12}(t) = -\Pi_{12}(t) + \mathrm{We}\,\Pi_{22}(t),$$

$$\dot{\Pi}_{11}(t) = -\Pi_{11}(t) + 2\,\mathrm{We}\,\Pi_{12}(t),$$

where

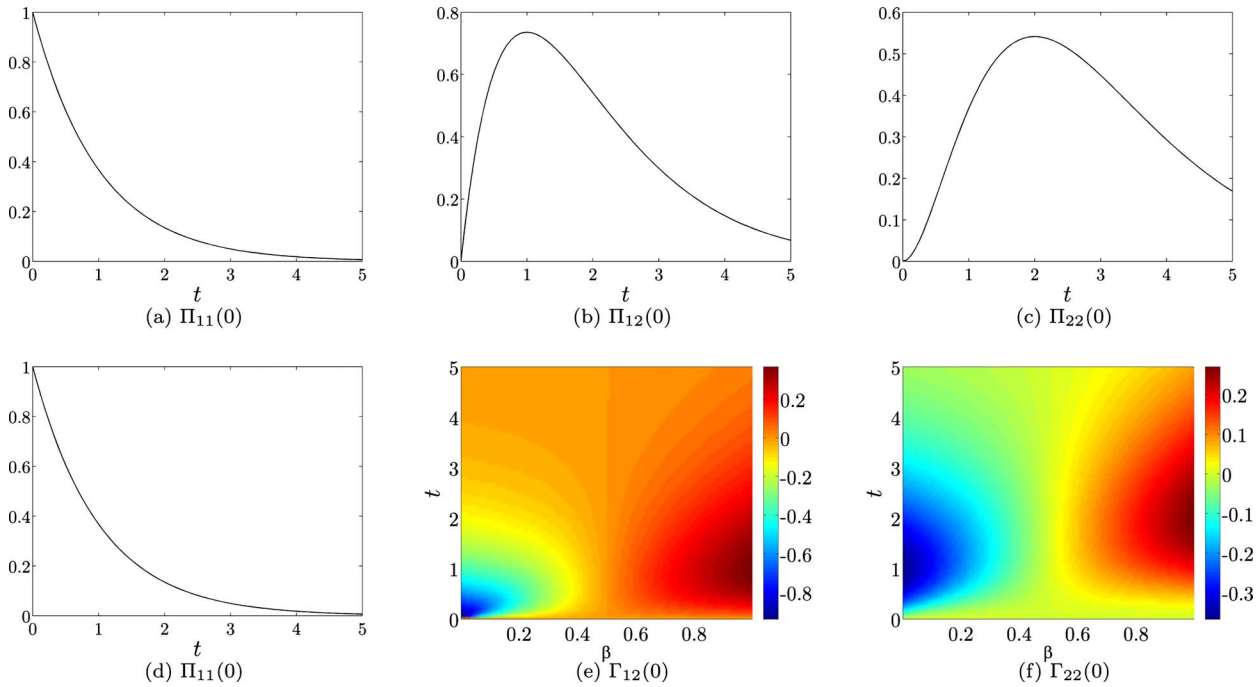

FIG. 13. (Color online) Functions mapping the initial conditions in (a) $\Pi_{11}(0)$, (b) $\Pi_{12}(0)$, (c) $\Pi_{22}(0)$, (d) $\Pi_{11}(0)$, (e) $\Gamma_{12}(0)$, and (f) $\Gamma_{22}(0)$ to $\Pi_{11}(t)$ in Couette (first row) and Poiseuille (second row) flows with We=1.

$$\Pi_{12}(t) = \frac{1}{2}\int_{-1}^{1} \tau_{12}(y,t)\mathrm{d}y.$$

The Laplace transform can now be utilized to obtain the expression for Π_{11},

$$\Pi_{11}(s) = \frac{1}{s+1}\Pi_{11}(0) + \frac{2\,\mathrm{We}}{(s+1)^2}\Pi_{12}(0) + \frac{2\,\mathrm{We}^2}{(s+1)^3}\Pi_{22}(0),$$

or equivalently in the time domain

$$\Pi_{11}(t) = \mathrm{e}^{-t}\Pi_{11}(0) + 2\,\mathrm{We}\,t\,\mathrm{e}^{-t}\Pi_{12}(0) + \mathrm{We}^2\,t^2\mathrm{e}^{-t}\Pi_{22}(0).$$

Therefore, in Couette flow, nonzero initial conditions in Π_{22} introduce an $\mathcal{O}(\mathrm{We}^2)$ response of $\Pi_{11}(t)$. This response is β-independent and it exhibits a temporal transient growth that achieves its maximum at $t=2$. We note that this large response is caused by the coupling from τ_{22} to τ_{12} and from τ_{12} to τ_{11}; physically, both these coupling terms represent stretching of polymer stress fluctuations by a background shear [cf. Eq. (19)].

On the other hand, the wall-normal integration of Eq. (19) in Poiseuille flow (see Appendix D) gives

$$\dot{\Gamma}_{22}(t) = -\Gamma_{22}(t),$$

$$\dot{\Gamma}_{12}(t) = -(1/\beta)\Gamma_{12}(t) + \mathrm{We}\,\Gamma_{22}(t),$$

$$\dot{\Pi}_{11}(t) = -\Pi_{11}(t) + \mathrm{We}(2-1/\beta)\Gamma_{12}(t),$$

where $\Gamma_{12}(t)$ and $\Gamma_{22}(t)$ are, respectively, determined by the first and second moments of τ_{12} and τ_{22},

$$\Gamma_{12}(t) = -2\int_{-1}^{1} y\tau_{12}(y,t)\mathrm{d}y,$$

$$\Gamma_{22}(t) = 4\int_{-1}^{1} y^2\tau_{22}(y,t)\mathrm{d}y.$$

The Laplace transform of the above equations can now be used to obtain

$$\Pi_{11}(s) = \frac{1}{s+1}\left(\Pi_{11}(0) + \frac{\mathrm{We}(2-1/\beta)}{s+1/\beta}\Gamma_{12}(0) + \frac{\mathrm{We}^2(2-1/\beta)}{(s+1)(s+1/\beta)}\Gamma_{22}(0)\right),$$

or equivalently in the time domain

$$\Pi_{11}(t) = \mathrm{e}^{-t}\Pi_{11}(0) + \mathrm{We}\frac{1-2\beta}{1-\beta}(\mathrm{e}^{-t/\beta} - \mathrm{e}^{-t})\Gamma_{12}(0) + \mathrm{We}^2\frac{2\beta-1}{(1-\beta)^2}[\beta(\mathrm{e}^{-t/\beta} - \mathrm{e}^{-t}) + (1-\beta)t\mathrm{e}^{-t}]\Gamma_{22}(0).$$

Thus, in Poiseuille flow, nonzero initial conditions in Γ_{22} introduce an $\mathcal{O}(\mathrm{We}^2)$ response of $\Pi_{11}(t)$. Contrary to Couette flow, this response exhibits a temporal transient growth that is β-dependent. Figure 13 shows contributions of different components of the polymer stress tensor at $t=0$ to $\Pi_{11}(t)$ in flows with We=1.

B. Transient growth of polymer stress fluctuations

In Sec. IV A, we have considered the transient response of elastic energy stored in infinitesimal polymer stress fluctuations. In this section, we study the transient growth of different components of the polymer stress fluctuation tensor. In particular, we show that the initial conditions in $\boldsymbol{\tau}_1$ and $\boldsymbol{\tau}_2$,

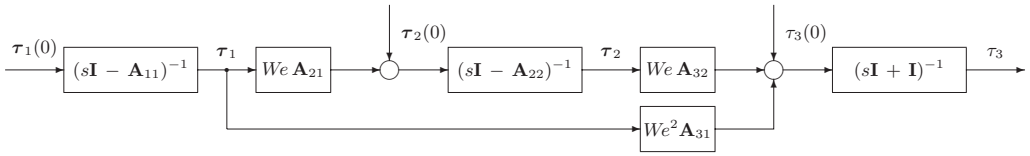

FIG. 14. The block diagram of streamwise-constant creeping flows of Oldroyd-B fluids, cf. Eq. (6). The initial conditions in $\boldsymbol{\tau}_1$ and $\boldsymbol{\tau}_2$, respectively, introduce $\mathcal{O}(\mathrm{We}^2)$ and $\mathcal{O}(\mathrm{We})$ responses of the streamwise component of the polymer stress tensor, $\tau_3=\tau_{11}$.

respectively, lead to $\mathcal{O}(\mathrm{We}^2)$ and $\mathcal{O}(\mathrm{We})$ responses of the streamwise component of the polymer stress tensor, $\tau_3=\tau_{11}$. This transient growth takes place on $\mathcal{O}(\mathrm{We})$ time scales and it is caused by the stretching of polymer stress fluctuations by a background shear.

The time evolution of $\boldsymbol{\tau}_1$ and $\boldsymbol{\tau}_2$ is captured by Eq. (9) in Sec. III B. On the other hand, system (6), which governs the dynamics of infinitesimal polymer stress fluctuations in streamwise-constant creeping flows of Oldroyd-B fluids, can be equivalently represented by the block diagram in Fig. 14. From this block diagram it is easy to see that τ_3 can be written as

$$\begin{aligned}\tau_3(y,k_z,t) = {} & \mathrm{We}^2[\mathbf{S}_{31}(k_z,t)\boldsymbol{\tau}_1(\cdot,k_z,0)](y) \\ & + \mathrm{We}[\mathbf{S}_{32}(k_z,t)\boldsymbol{\tau}_2(\cdot,k_z,0)](y) \\ & + [\mathbf{S}_{33}(k_z,t)\tau_3(\cdot,k_z,0)](y),\end{aligned}$$

where the We-independent operators $\mathbf{S}_{3i}$ describe how the initial conditions in $\boldsymbol{\tau}_i$ influence the temporal evolution of τ_3 for each $i=\{1,2,3\}$. This expression implies that $\tau_3(0)$ induces a We-independent response of τ_3; on the other hand, $\boldsymbol{\tau}_1(0)$ and $\boldsymbol{\tau}_2(0)$ trigger responses of τ_3 that are proportional to We^2 and We, respectively. Thus, in strongly elastic creeping flows of viscoelastic fluids the influence of initial conditions in $\boldsymbol{\tau}_1$ should be most pronounced; the presence of $\boldsymbol{\tau}_1(0)$ has the strongest, i.e., $\mathcal{O}(\mathrm{We}^2)$, effect on the streamwise component of the polymer stress tensor, $\tau_3=\tau_{11}$. We also note that this We^2-scaling of τ_3 comes from operators $\mathbf{A}_{21}$, $\mathbf{A}_{31}$, and $\mathbf{A}_{32}$ (see Fig. 14), and that each of these operators contains polymer stretching as its integral part (for definitions of these operators, see Eq. (A3) and Sec. II B).

Since $\boldsymbol{\tau}_1(0)$ sets up an $\mathcal{O}(\mathrm{We}^2)$ response of $\tau_3(t)$, we next examine the maximal transient growth of τ_3 (as a function of k_z, t, and β) that comes from $\boldsymbol{\tau}_1(0)$. For any fixed $(\mathrm{We},\beta;k_z,t)$, this quantity is determined by

$$\begin{aligned}G_{31}(\mathrm{We},\beta;k_z,t) &= \sup_{\boldsymbol{\tau}_1(0)\neq 0,\ \boldsymbol{\tau}_2(0)\equiv 0,\ \tau_3(0)\equiv 0} \frac{\|\tau_3(\cdot,k_z,t)\|_2^2}{\|\boldsymbol{\tau}_1(\cdot,k_z,0)\|_2^2} \\ &= \sup_{\|\boldsymbol{\tau}_1(0)\|_2=1,\ \boldsymbol{\tau}_2(0)\equiv 0,\ \tau_3(0)\equiv 0} \|\tau_3(\cdot,k_z,t)\|_2^2 \\ &= \mathrm{We}^4\sigma_{\max}(\mathbf{S}_{31}(\beta;k_z,t)) \\ &= \mathrm{We}^4\bar{G}_{31}(\beta;k_z,t). \qquad (20)\end{aligned}$$

Figure 15 illustrates the maximal transient growth of the streamwise component of the polymer stress tensor, $\tau_3=\tau_{11}$, arising from the initial conditions in $\boldsymbol{\tau}_1$ in flows with $\beta=0.1$, $\bar{G}_{31}(0.1;k_z,t)$. For each value of k_z we observe two transient growth peaks in Couette flow and a single peak in Poiseuille flow. Contrary to the results of Sec. III, the transient response of τ_{11} is fairly flat in k_z and without a high-wavenumber roll-off, which reflects the absence of diffusion terms in Eq. (6). The absence of stress diffusion in constitutive equations describing rheological properties of viscoelastic fluids is well documented (see, for example, Refs. 27 and 47–50). Our numerical computations indicate that the addition of a small amount of diffusion to the constitutive equations, i.e., the addition of a term $d\Delta\mathbf{T}$ to the right-hand side of Eq. (1c) (as commonly done in direct numerical simulations of viscoelastic fluids), introduces a high-wavenumber roll-off in the transient response of polymer stress fluctuations [cf. Figs. 15(a) and 16(b)]; on the other hand, the transient response of velocity fluctuations remains impervious to this addition [cf. Figs. 3(a) and 16(a)]. Figure 16 illustrates the transient growth of u and τ_{11} arising from the initial conditions in $\boldsymbol{\tau}_1$ in Couette flow with $\beta=0.1$ and $d=10^{-3}$. Results in Poiseuille flow exhibit similar trends and are not reported here for brevity. We note that diffusion in constitutive equations can be obtained by accounting for the influence of Brownian motion on the center of mass of the Hookean dumbbells representing polymer molecules.[47]

It is worth noting that in Couette flow with $k_x=k_z=0$, the transient growth function $\bar{G}_{31}(\beta;0,t)$ can be determined explicitly. As shown in Appendix D, the dynamics of the streamwise component of the polymer stress tensor τ_{11} in Couette flow with $k_x=k_z=0$ are governed by [cf. Eq. (D1)]

$$\dot{\tau}_{22} = -\tau_{22},$$

$$\dot{\tau}_{12} = -(1/\beta)\tau_{12} + (1/\beta - 1)\Pi_{12}(t) + \mathrm{We}\,\tau_{22},$$

$$\dot{\tau}_{11} = -\tau_{11} + 2\,\mathrm{We}[(1/\beta - 1)\Pi_{12}(t) + (2 - 1/\beta)\tau_{12}].$$

The application of the Laplace transform to this system of equations yields the following expression for τ_{11}:

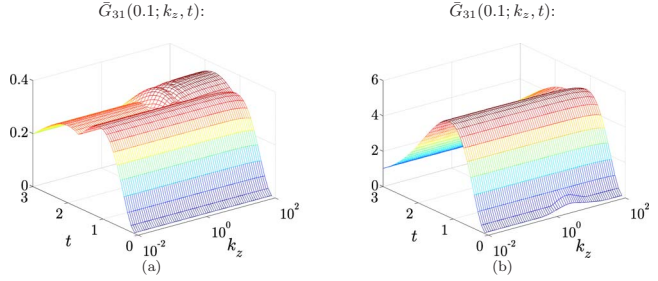

FIG. 15. (Color online) Maximal transient growth of the streamwise component of the polymer stress tensor $\tau_3=\tau_{11}$ in (a) Couette and (b) Poiseuille flows with $\beta=0.1$ arising from the initial condition in $\boldsymbol{\tau}_1$. All other initial conditions have been set to zero.

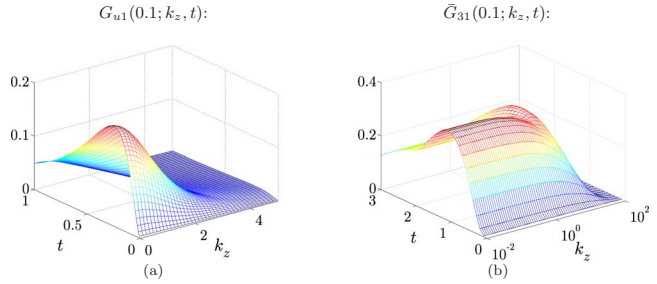

FIG. 16. (Color online) Maximal transient growth of (a) the streamwise velocity fluctuation u and (b) the streamwise component of the polymer stress fluctuation tensor $\tau_3=\tau_{11}$ in Couette flow with $\beta=0.1$ and $d=10^{-3}$, arising from the initial condition in $\boldsymbol{\tau}_1$. All other initial conditions have been set to zero.

$$\tau_{11}(y,s)=\frac{1}{s+1}\tau_{11}(y,0)+\mathrm{We}(s+1)(h_1(s)\Pi_{12}(0)-h_2(s)\tau_{12}(y,0))+\mathrm{We}^2(h_1(s)\Pi_{22}(0)-h_2(s)\tau_{22}(y,0)).$$

Here,

$$h_1(s)=\frac{2(1-\beta)(s+2)}{(\beta s+1)(s+1)^3},\quad h_2(s)=\frac{2(1-2\beta)}{(\beta s+1)(s+1)^2},$$

or equivalently in the time domain,

$$h_1(t)=(\{\beta^2(t+2)^2-2\beta[t(t+3)+1]+t(t+2)\}\mathrm{e}^{-t}+2(1-2\beta)\beta\mathrm{e}^{-t/\beta})/(1-\beta)^2,$$
$$h_2(t)=2(1-2\beta)\{\beta\mathrm{e}^{-t/\beta}+[t-\beta(t+1)]\mathrm{e}^{-t}\}/(1-\beta)^2. \quad (21)$$

It is now easy to show that the $L_2[-1,1]$ norm of τ_{11} arising from the initial conditions in τ_{22} is determined by the following linear combination of $\Pi_{22}^2(0)$ and the L_2 norm of $\tau_{22}(0)$:

$$\|\tau_{11}(\cdot,t)\|_2^2=\mathrm{We}^4\{h_2^2(t)\|\tau_{22}(\cdot,0)\|_2^2+2h_1(t)\times[h_1(t)-2h_2(t)]\Pi_{22}^2(0)\}.$$

Using Eq. (20) and the fact that the only component of $\boldsymbol{\tau}_1(y,0)$ that influences $\tau_{11}(y,t)$ at $k_z=0$ is $\tau_{22}(y,0)$, we conclude that

$$\bar{G}_{31}(\beta;0,t)=\sup_{\|\tau_{22}(0)\|_2=1,\ \tau_{11}(0)=\tau_{12}(0)\equiv 0}\|\tau_{11}(\cdot,t)\|_2^2|_{\mathrm{We}=1}.$$

Thus, the transient growth function $\bar{G}_{31}(\beta;0,t)$ for times at which $h_1(t)[h_1(t)-2h_2(t)]\le 0$ is determined by $\bar{G}_{31}(\beta;0,t)=h_2^2(t)$. On the other hand, for times at which function $h_1(t)[h_1(t)-2h_2(t)]$ is positive we have

$$\bar{G}_{31}(\beta;0,t)=\sup_{\|\tau_{22}(0)\|_2=1,\ \tau_{11}(0)=\tau_{12}(0)\equiv 0}\{h_2^2(t)\|\tau_{22}(\cdot,0)\|_2^2+2h_1(t)[h_1(t)-2h_2(t)]\Pi_{22}^2(0)\}.$$

Now, we can use the Cauchy–Schwarz inequality to upper bound $\Pi_{22}^2(0)$,

$$\Pi_{22}^2(0)=\tfrac{1}{4}\langle\tau_{22}(\cdot,0),1\rangle^2\le\tfrac{1}{4}\|\tau_{22}(\cdot,0)\|_2^2\|1\|_2^2=\tfrac{1}{2}\|\tau_{22}(\cdot,0)\|_2^2.$$

For unit norm initial condition $\tau_{22}(y,0)$, $\|\tau_{22}(\cdot,0)\|_2=1$, this upper bound on $\Pi_{22}^2(0)$ is strict [i.e., it can be achieved with $\tau_{22}(y,0)=1/\sqrt{2}$]. Therefore, if $h_1(t)[h_1(t)-2h_2(t)]>0$ then $\bar{G}_{31}(\beta;0,t)=h_2^2(t)+h_1(t)[h_1(t)-2h_2(t)]$. A bit of algebra can be used to simplify this expression for $\bar{G}_{31}(\beta;0,t)$, which finally yields $h_2^2(t)+h_1(t)[h_1(t)-2h_2(t)]=t^4\mathrm{e}^{-2t}$. Alternatively, this formula for $\bar{G}_{31}(\beta;0,t)$ can readily be obtained from Eq. (19). Namely, in Couette flow with $\{\tau_{22}(y,0)=1/\sqrt{2};\tau_{12}(y,0)=\tau_{11}(y,0)\equiv 0\}$, Eq. (C4) implies that $u(y,t)\equiv 0$ and, thus, Eq. (19) simplifies to

$$\dot{\tau}_{22}=-\tau_{22},$$

$$\dot{\tau}_{12}=-\tau_{12}+\mathrm{We}\,\tau_{22},$$

$$\dot{\tau}_{11}=-\tau_{11}+2\,\mathrm{We}\,\tau_{12}.$$

It is now straightforward to determine the response of τ_{11} caused by the initial condition in τ_{22}, $\tau_{11}(y,t)=\mathrm{We}^2t^2\mathrm{e}^{-t}\tau_{22}(y,0)$, which consequently leads to the above expression for $\bar{G}_{31}(\beta;0,t)$.

To recap, in Couette flow with $k_x=k_z=0$ the transient growth function $\bar{G}_{31}(\beta;0,t)$ is determined by

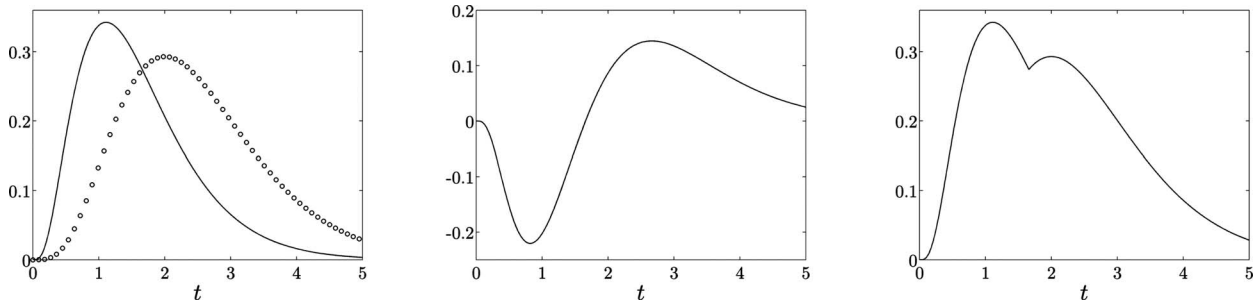

(a) $h_2^2(t)$ (solid), $t^4\,\mathrm{e}^{-2t}$ (circles) (b) $h_1(t)\,(h_1(t)-2h_2(t))$ (c) $\bar{G}_{31}(0.1;0,t)$

FIG. 17. The time dependence of functions (a) $h_2^2(t)$ (solid), $t^4\mathrm{e}^{-2t}$ (circles); (b) $h_1(t)[h_1(t)-2h_2(t)]$; and (c) $\bar{G}_{31}(0.1;0,t)$ in Couette flow with $\beta=0.1$ and $k_z=0$.

$$\bar{G}_{31}(\beta;0,t) = \sup_{\|\tau_{22}(0)\|_2=1,\ \tau_{11}(0)=\tau_{12}(0)\equiv 0} \|\tau_{11}(\cdot,t)\|_2^2|_{\mathrm{We}=1}$$
$$= \begin{cases} h_2^2(t), & h_1(t)[h_1(t)-2h_2(t)] \le 0, \\ t^4 e^{-2t}, & h_1(t)[h_1(t)-2h_2(t)] > 0, \end{cases}$$

where $h_1(t)$ and $h_2(t)$ are given by Eq. (21). Figure 17 illustrates the functions $h_2^2(t)$, t^4e^{-2t}, $h_1(t)[h_1(t)-2h_2(t)]$, and $\bar{G}_{31}(0.1;0,t)$ in Couette flow with $\beta=0.1$. Our analytical results agree with the above numerical computations [cf. Fig. 15(a) for small values of k_z] and justify the existence of the "kinks" observed in Fig. 15(a). These take place because of the existence of a time instant at which function $h_1(t)[h_1(t)-2h_2(t)]$ vanishes [for illustration at $\beta=0.1$, see Fig. 17(b)]; at this value of t, the transient growth function changes its character from $h_2^2(t)$ to t^4e^{-2t} [cf. Fig. 17(c)].

V. CONCLUDING REMARKS

We have studied transient responses of velocity and polymer stress fluctuations in inertialess channel flows of Oldroyd-B fluids. By focusing on the analysis of streamwise-constant fluctuations, we are able to obtain a number of new analytical results. In contrast, most prior work on this topic has focused on the analysis of spanwise-constant fluctuations, which does not yield analytical results as readily and is prone to numerical difficulties in high-Weissenberg-number flows.[27] In addition, both velocity and polymer stress fluctuations may be nonzero in our work, which sets it apart from a recent paper that considered only nonzero (but 3D) polymer stress fluctuations in an upper convected Maxwell fluid.[29]

We have shown that both velocity and polymer stress fluctuations may experience a significant transient growth. For velocity fluctuations, the streamwise component u is most sensitive to elasticity and it exhibits an $\mathcal{O}(\mathrm{We})$ growth over an $\mathcal{O}(\mathrm{We})$ time scale before eventually decaying. This growth arises from the initial conditions in the wall-normal/spanwise polymer stress components [i.e., $\tau_{22}(0)$, $\tau_{23}(0)$, and $\tau_{33}(0)$], with $\tau_{22}(0)$ generating the largest contribution. Our results indicate that the Oldroyd-B model is not capable of selecting a preferential spanwise length scale in flows subject to only $\tau_{22}(0)$; this is a consequence of the fact that the largest transient growth of $u(t)$ caused by $\tau_{22}(0)$ takes place at zero spanwise wave number k_z. On the other hand, the transient growth peaks of streamwise velocity fluctuations arising from the initial conditions in τ_{23} and τ_{33} occur at $\mathcal{O}(1)$ values of k_z. This suggests that the length scale selection in experiments may very much be influenced by the initial distribution of the polymer stress fluctuations and by the presence of physical boundaries and background disturbances in a laboratory setup. It is also striking that for streamwise-constant fluctuations, creeping flows of viscoelastic fluids have velocity fluctuation dynamics that are structurally similar to those of inertial flows of Newtonian fluids, with the Weissenberg number playing the role of the Reynolds number [cf. block diagrams in Figs. 12(a) and 12(b)]. In Newtonian fluids, vortex tilting is the underlying mechanism for transient growth, whereas in viscoelastic fluids, we have shown that it is polymer stretching by a background shear which produces large transient responses. For polymer stress fluctuations, the streamwise component τ_{11} is most sensitive to elasticity, exhibiting an $\mathcal{O}(\mathrm{We}^2)$ growth over an $\mathcal{O}(\mathrm{We})$ time scale, with polymer stretching once again being the culprit behind the observed transient growth. Our analysis shows that the transient response of τ_{11} is fairly flat in k_z with a high-wavenumber roll-off being observed only upon inclusion of a small amount of stress diffusion in the constitutive equations. We note that this addition does not have a pronounced influence on the transient behavior of velocity fluctuations.

The present work makes clear that streamwise-constant fluctuations in channel flows of viscoelastic fluids can undergo a significant transient growth even in the absence of inertia. It also reveals remarkable similarities between inertial flows of Newtonian fluids and creeping flows of Oldroyd-B fluids. Since prior work has identified that spanwise-constant fluctuations can also experience a considerable transient growth, this raises the question of the structure of flow fluctuations that grow most robustly in practice. Direct numerical simulations and experimental studies of the early stages of transition in wall-bounded shear flows of dilute polymer solutions would provide insight into this question, and observations made in this paper may provide guidance in interpreting the results of such investigations.

ACKNOWLEDGMENTS

This work was partially supported by the National Science Foundation under CAREER Award No. CMMI-06-44793 (to M.R.J.), by the Department of Energy under Award No. DE-FG02-07ER46415 (to S.K.), and by the University of Minnesota Digital Technology Center's 2010 Digital Technology Initiative Seed Grant (to M.R.J. and S.K.).

APPENDIX A: DYNAMICS OF THE STREAMWISE-CONSTANT FLOW FLUCTUATIONS

In this appendix we describe the equations governing the evolution of streamwise-constant flow fluctuations in creeping flows of an Oldroyd-B fluid. We also define the underlying operators in Eqs. (5)–(7).

By decomposing the velocity, pressure, and polymer stress fields into the sum of base and fluctuating parts (i.e., $\mathbf{V}=\bar{\mathbf{v}}+\mathbf{v}$, $P=\bar{P}+p$, and $\mathbf{T}=\bar{\boldsymbol{\tau}}+\boldsymbol{\tau}$), Eqs. (2), (1b), and (1c) can be brought to the form

$$0 = \beta\Delta\mathbf{v} + (1-\beta)\nabla\cdot\boldsymbol{\tau} - \nabla p, \tag{A1a}$$

$$0 = \nabla\cdot\mathbf{v}, \tag{A1b}$$

$$\dot{\boldsymbol{\tau}} = \mathcal{L}(\boldsymbol{\tau},\mathbf{v}) + \mathcal{N}(\boldsymbol{\tau},\mathbf{v}), \tag{A1c}$$

where $\mathcal{L}(\boldsymbol{\tau},\mathbf{v})$ and $\mathcal{N}(\boldsymbol{\tau},\mathbf{v})$, respectively, denote linear and nonlinear flow fluctuation terms, i.e.,

$$\mathcal{L}(\boldsymbol{\tau},\mathbf{v}) = \nabla\mathbf{v} + (\nabla\mathbf{v})^T - \boldsymbol{\tau} - \mathrm{We}(\mathbf{v}\cdot\nabla\bar{\boldsymbol{\tau}} + \bar{\mathbf{v}}\cdot\nabla\boldsymbol{\tau})$$
$$+ \mathrm{We}(\boldsymbol{\tau}\cdot\nabla\bar{\mathbf{v}} + (\boldsymbol{\tau}\cdot\nabla\bar{\mathbf{v}})^T + \bar{\boldsymbol{\tau}}\cdot\nabla\mathbf{v} + (\bar{\boldsymbol{\tau}}\cdot\nabla\mathbf{v})^T),$$

$$\mathcal{N}(\boldsymbol{\tau},\mathbf{v}) = \mathrm{We}[\boldsymbol{\tau}\cdot\nabla\mathbf{v} + (\boldsymbol{\tau}\cdot\nabla\mathbf{v})^T - \mathbf{v}\cdot\nabla\boldsymbol{\tau}].$$

The linearized dynamics are obtained by neglecting quadratic term $\mathcal{N}(\boldsymbol{\tau},\mathbf{v})$ in Eq. (A1c). For purely harmonic fluctuations in the spanwise direction, e.g.,

$$\mathbf{v}(y,z,t) = \Re[\mathbf{v}(y,k_z,t)\mathrm{e}^{\mathrm{i}k_z z}],$$

the linearized evolution model is given by Eq. (5). Here, $\Re(\cdot)$ denotes the real part of a given quantity, and the **F**-operators in Eq. (4) are given by

$$\mathbf{F}_{1\psi} = \begin{bmatrix} 2\mathrm{i}k_z\partial_y & -(\partial_{yy}+k_z^2) & -2\mathrm{i}k_z\partial_y \end{bmatrix}^T,$$

$$\mathbf{F}_{2\psi} = \begin{bmatrix} \mathrm{i}k_z(U'(y)\partial_y - U''(y)) \\ -U'(y)\partial_{yy} \end{bmatrix}, \quad \mathbf{F}_{2u} = \begin{bmatrix} \partial_y \\ \mathrm{i}k_z \end{bmatrix},$$

$$\mathbf{F}_{21} = \begin{bmatrix} U'(y) & 0 & 0 \\ 0 & U'(y) & 0 \end{bmatrix}, \quad \mathbf{F}_{3\psi} = -4\mathrm{i}k_z U'(y)U''(y), \tag{A2}$$

$$\mathbf{F}_{3u} = 2U'(y)\partial_y, \quad \mathbf{F}_{32} = \begin{bmatrix} 2U'(y) & 0 \end{bmatrix}.$$

Substitution of Eq. (3) into Eq. (5) leads to the set of evolution equations (6) for the polymer stress components with the **A**-operators given by

$$\mathbf{A}_{11} = -\mathbf{I} + \mathbf{F}_{1\psi}\mathbf{C}_\psi, \quad \mathbf{A}_{22} = -\mathbf{I} + \mathbf{F}_{2u}\mathbf{C}_u,$$

$$\mathbf{A}_{21} = \mathbf{F}_{21} + \mathbf{F}_{2\psi}\mathbf{C}_\psi, \quad \mathbf{A}_{31} = \mathbf{F}_{3\psi}\mathbf{C}_\psi, \quad \mathbf{A}_{32} = \mathbf{F}_{32} + \mathbf{F}_{3u}\mathbf{C}_u. \tag{A3}$$

The **C**-operators appearing in Eq. (7), which is convenient for quantifying the scaling of the kinetic energy density with the Weissenberg number, are given by

$$\mathbf{C}_u = -(1/\beta - 1)\Delta^{-1}\begin{bmatrix} \partial_y & \mathrm{i}k_z \end{bmatrix}, \quad \mathbf{C}_v = \mathrm{i}k_z\mathbf{C}_\psi,$$

$$\mathbf{C}_w = -\partial_y\mathbf{C}_\psi, \tag{A4}$$

where $\mathbf{C}_\psi$ is defined in Eq. (4). The expressions for operators $\mathbf{C}_v$ and $\mathbf{C}_w$ are obtained by substituting $\psi = \mathbf{C}_\psi\boldsymbol{\tau}_1$ [cf. Eq. (3)] into the equation relating the wall-normal and spanwise velocity fluctuations with the streamfunction, $\{v = \mathrm{i}k_z\psi, \ w = -\partial_y\psi\}$.

APPENDIX B: OPERATORS $\mathbf{C}_u$ AND $\mathbf{H}_{1r}$ AT LARGE AND SMALL VALUES OF k_z

We next briefly discuss the properties of $\mathbf{C}_u$ and $\mathbf{H}_{1r}$ at large and small values of k_z. From Eqs. (4) and (15) we recall that these operators are given by

$$\mathbf{C}_u = -\frac{1-\beta}{\beta}\Delta^{-1}\begin{bmatrix} \partial_y & \mathrm{i}k_z \end{bmatrix},$$

$$\mathbf{H}_{1a} = -\frac{1-\beta}{\beta}\Delta^{-1}\begin{bmatrix} U''(y) + U'(y)\partial_y & \mathrm{i}k_z U'(y) & 0 \end{bmatrix},$$

$$\mathbf{H}_{1b} = \frac{(1-\beta)^2}{\beta^2}\mathrm{i}k_z\Delta^{-1}[2U''(y)\partial_y + U'(y)\Delta] \times \Delta^{-2}\begin{bmatrix} \mathrm{i}k_z\partial_y & -(\partial_{yy}+k_z^2) & -\mathrm{i}k_z\partial_y \end{bmatrix}.$$

At $k_z = 0$, operator $\mathbf{H}_{1b}$ becomes identically equal to zero, whereas $\mathbf{C}_u$ and $\mathbf{H}_{1a}$ simplify to

$$\mathbf{C}_u(k_z=0) = -(1/\beta - 1)\partial_{yy}^{-1}\begin{bmatrix} \partial_y & 0 \end{bmatrix},$$

$$\mathbf{H}_{1a}(k_z=0) = -(1/\beta - 1)\partial_{yy}^{-1}\begin{bmatrix} U''(y) + U'(y)\partial_y & 0 & 0 \end{bmatrix}.$$

These observations in conjunction with Eq. (16) imply that at $k_z = 0$, only the initial conditions in τ_{12} and τ_{22} contribute to the response of streamwise velocity fluctuations. On the other hand, in the limit of infinitely large values of k_z, the influence of both $\mathbf{C}_u$ and $\mathbf{H}_{1r}$ becomes negligibly small. This is because operators Δ^{-1} and Δ^{-2} at large k_z approximately scale as $1/k_z^2$ and $1/k_z^4$, respectively, which implies that

$$\lim_{k_z\to\infty}[\mathbf{C}_u\boldsymbol{\tau}_2(\cdot,k_z,0)](y) = 0, \quad \lim_{k_z\to\infty}[\mathbf{H}_{1r}\boldsymbol{\tau}_1(\cdot,k_z,0)](y) = 0.$$

Now, using Eq. (16), we conclude that $\lim_{k_z\to\infty} u(y,k_z,t) = 0$.

APPENDIX C: LINEARIZED EQUATIONS AT $k_z = 0$

Motivated by the observation that the largest transient growth of streamwise-constant fluctuations takes place at $k_z = 0$ (cf. Sec. III C), we examine the linearized model with $k_x = k_z = 0$. In this case, the continuity equation simplifies to $\partial_y v = 0$, which—in view of homogeneous Dirichlet boundary conditions on v—implies that $v(y,t) \equiv 0$. Furthermore, the linearized momentum and constitutive equations are, respectively, given by

$$\beta\partial_{yy}u = -(1-\beta)\partial_y\tau_{12},$$

$$\beta\partial_{yy}w = -(1-\beta)\partial_y\tau_{23}, \tag{C1}$$

$$\partial_y p = (1-\beta)\partial_y\tau_{22}$$

and

$$\dot{\boldsymbol{\tau}}_1 = -\boldsymbol{\tau}_1 + \begin{bmatrix} 0 \\ \partial_y \\ 0 \end{bmatrix} w, \tag{C2a}$$

$$\dot{\boldsymbol{\tau}}_2 = -\boldsymbol{\tau}_2 + \begin{bmatrix} \partial_y \\ 0 \end{bmatrix} u + \mathrm{We}\left(\begin{bmatrix} 0 \\ U'(y)\partial_y \end{bmatrix} w + \begin{bmatrix} U'(y) & 0 & 0 \\ 0 & U'(y) & 0 \end{bmatrix}\boldsymbol{\tau}_1 \right), \tag{C2b}$$

$$\dot{\tau}_3 = -\tau_3 + 2\,\mathrm{We}\left(U'(y)\partial_y u + \begin{bmatrix} U'(y) & 0 \end{bmatrix}\boldsymbol{\tau}_2\right). \tag{C2c}$$

Following the procedure outlined in Sec. III C, we obtain

$$w(s) = \frac{-(1/\beta - 1)}{s + 1/\beta}\partial_{yy}^{-1}\partial_y\tau_{23}(0),$$

or equivalently in the time domain,

$$w(y,t) = -(1/\beta - 1)\mathrm{e}^{-t/\beta}[\partial_{yy}^{-1}\partial_y\tau_{23}(\cdot,0)](y). \tag{C3}$$

Similarly, the streamwise velocity can be expressed as

$$u(s) = \mathrm{We}\,u_{22}(s) + u_{12}(s),$$

$$u_{12}(s) = \frac{-(1/\beta - 1)}{s + 1/\beta}\partial_{yy}^{-1}\partial_y\tau_{12}(0),$$

$$u_{22}(s) = \frac{-(1/\beta - 1)}{(s + 1/\beta)(s+1)} \partial_{yy}^{-1}[U''(y) + U'(y)\partial_y]\tau_{22}(0),$$

or equivalently in the time domain,

$$u(y,t) = \mathrm{We}\, u_{22}(y,t) + u_{12}(y,t),$$

$$u_{12}(y,t) = -(1/\beta - 1)\mathrm{e}^{-t/\beta}[\partial_{yy}^{-1}\partial_y \tau_{12}(\cdot,0)](y), \tag{C4}$$

$$u_{22}(y,t) = -(\mathrm{e}^{-t} - \mathrm{e}^{-t/\beta})[\partial_{yy}^{-1}(U''(y) + U'(y)\partial_y)\tau_{22}(\cdot,0)](y).$$

Now, from Eqs. (C1), (C3), and (C4) we conclude that

$$w(y,t) = \mathrm{e}^{-t/\beta} w(y,0), \quad u_{12}(y,t) = \mathrm{e}^{-t/\beta} u(y,0),$$

which implies that the initial conditions in the streamwise and the spanwise velocity create monotonically decaying We-independent responses of $u(y,t)$ and $w(y,t)$, with a rate of decay inversely proportional to the viscosity ratio β. On the other hand, even though $\tau_{22}(y,0) \neq 0$ yields zero initial kinetic energy,[51] the presence of initial conditions in τ_{22} generates streamwise velocity fluctuations, We $u_{22}(y,t)$, which scale linearly with the Weissenberg number and also exhibit temporal transient growth. We note that this feature arises solely due to viscoelastic nature of the underlying fluid.

APPENDIX D: ELASTIC ENERGY OF POLYMER STRESS FLUCTUATIONS IN POISEUILLE FLOW

Here we examine the contribution of τ_{11} to the elastic energy in Poiseuille flow. Before we turn our attention to Eq. (19), we note that Eq. (C1), in conjunction with Dirichlet boundary conditions on u, can be used to obtain

$$\partial_y u(y,t) = (1/\beta - 1)[\Pi_{12}(t) - \tau_{12}(y,t)],$$

which in turn implies

$$\partial_y u(y,t) + \tau_{12}(y,t) = (1/\beta - 1)\Pi_{12}(t) + (2 - 1/\beta)\tau_{12}(y,t),$$

$$\partial_y u(y,t) - \tau_{12}(y,t) = (1/\beta - 1)\Pi_{12}(t) - (1/\beta)\tau_{12}(y,t).$$

Substitution of these two auxiliary equalities to Eq. (19) yields

$$\dot{\tau}_{22} = -\tau_{22}, \tag{D1a}$$

$$\dot{\tau}_{12} = -(1/\beta)\tau_{12} + (1/\beta - 1)\Pi_{12}(t) + \mathrm{We}\, U'(y)\tau_{22}, \tag{D1b}$$

$$\dot{\tau}_{11} = -\tau_{11} + 2\,\mathrm{We}\, U'(y)[(1/\beta - 1)\Pi_{12}(t) + (2 - 1/\beta)\tau_{12}]. \tag{D1c}$$

We note that Eq. (D1) is valid in both Couette and Poiseuille flows. In particular, in Poiseuille flow $U(y) = 1 - y^2$ and the wall-normal integration of Eq. (D1c) thus yields

$$\dot{\Pi}_{11}(t) = -\Pi_{11}(t) + \mathrm{We}(2 - 1/\beta)\Gamma_{12}(t),$$

where

$$\Gamma_{12}(t) = \int_{-1}^{1} U'(y)\tau_{12}(y,t)\mathrm{d}y.$$

Similarly, multiplication of Eqs. (D1a) and (D1b) by $U'(y)$ and subsequent integration in y gives

$$\dot{\Gamma}_{22}(t) = -\Gamma_{22}(t),$$

$$\dot{\Gamma}_{12}(t) = -(1/\beta)\Gamma_{12}(t) + \mathrm{We}\,\Gamma_{22}(t),$$

where

$$\Gamma_{22}(t) = \int_{-1}^{1} [U'(y)]^2 \tau_{22}(y,t)\mathrm{d}y.$$

The analysis of the temporal evolution of $\Pi_{11}(t)$ is given in Sec. IV A.

[1] R. G. Larson, "Turbulence without inertia," Nature (London) **405**, 27 (2000).
[2] A. Groisman and V. Steinberg, "Elastic turbulence in a polymer solution flow," Nature (London) **405**, 53 (2000).
[3] A. Groisman and V. Steinberg, "Elastic turbulence in curvilinear flows of polymer solutions," New J. Phys. **6**, 29 (2004).
[4] P. E. Arratia, C. C. Thomas, J. Diorio, and J. P. Gollub, "Elastic instabilities of polymer solutions in cross-channel flow," Phys. Rev. Lett. **96**, 144502 (2006).
[5] Y. Jun and V. Steinberg, "Power and pressure fluctuations in elastic turbulence over a wide range of polymer concentrations," Phys. Rev. Lett. **102**, 124503 (2009).
[6] B. Thomases and M. Shelley, "Transition to mixing and oscillations in a Stokesian viscoelastic flow," Phys. Rev. Lett. **103**, 094501 (2009).
[7] R. G. Larson, "Instabilities in viscoelastic flows," Rheol. Acta **31**, 213 (1992).
[8] R. G. Larson, *The Structure and Rheology of Complex Fluids* (Oxford University Press, New York, 1999).
[9] A. Groisman and V. Steinberg, "Efficient mixing at low Reynolds numbers using polymer additives," Nature (London) **410**, 905 (2001).
[10] J. M. Ottino and S. Wiggins, "Introduction: Mixing in microfluidics," Philos. Trans. R. Soc. London, Ser. A **362**, 923 (2004).
[11] S. Grossmann, "The onset of shear flow turbulence," Rev. Mod. Phys. **72**, 603 (2000).
[12] P. J. Schmid and D. S. Henningson, *Stability and Transition in Shear Flows* (Springer-Verlag, Berlin, 2001).
[13] P. J. Schmid, "Nonmodal stability theory," Annu. Rev. Fluid Mech. **39**, 129 (2007).
[14] K. M. Butler and B. F. Farrell, "Three-dimensional optimal perturbations in viscous shear flow," Phys. Fluids A **4**, 1637 (1992).
[15] L. N. Trefethen, A. E. Trefethen, S. C. Reddy, and T. A. Driscoli, "Hydrodynamic stability without eigenvalues," Science **261**, 578 (1993).
[16] B. F. Farrell and P. J. Ioannou, "Stochastic forcing of the linearized Navier–Stokes equations," Phys. Fluids A **5**, 2600 (1993).
[17] B. Bamieh and M. Dahleh, "Energy amplification in channel flows with stochastic excitations," Phys. Fluids **13**, 3258 (2001).
[18] M. R. Jovanović and B. Bamieh, "Componentwise energy amplification in channel flows," J. Fluid Mech. **534**, 145 (2005).
[19] L. N. Trefethen and M. Embree, *Spectra and Pseudospectra: The Behavior of Nonnormal Matrices and Operators* (Princeton University Press, Princeton, NJ, 2005).
[20] M. Matsubara and P. H. Alfredsson, "Disturbance growth in boundary layers subjected to free-stream turbulence," J. Fluid Mech. **430**, 149 (2001).
[21] D. S. Henningson, A. Lundbladh, and A. V. Johansson, "A mechanism for bypass transition from localized disturbances in wall-bounded shear flows," J. Fluid Mech. **250**, 169 (1993).
[22] R. G. Jacobs and P. A. Durbin, "Simulations of bypass transition," J. Fluid Mech. **428**, 185 (2001).
[23] L. Brandt, P. Schlatter, and D. S. Henningson, "Transition in boundary layers subject to free-stream turbulence," J. Fluid Mech. **517**, 167 (2004).
[24] G. B. Schubauer and H. F. Skramstad, "Laminar boundary layer oscillations and the stability of laminar flow," J. Aerosp. Sci. **14**, 69 (1947).
[25] R. Sureshkumar, M. D. Smith, R. C. Armstrong, and R. A. Brown, "Linear stability and dynamics of viscoelastic flows using time-dependent numerical simulations," J. Non-Newtonian Fluid Mech. **82**, 57 (1999).
[26] K. Atalik and R. Keunings, "Non-linear temporal stability analysis of viscoelastic plane channel flows using a fully spectral method," J. Non-Newtonian Fluid Mech. **102**, 299 (2002).
[27] R. Kupferman, "On the linear stability of plane Couette flow for an

Oldroyd-B fluid and its numerical approximation," J. Non-Newtonian Fluid Mech. **127**, 169 (2005).
[28]C. Doering, B. Eckhardt, and J. Schumacher, "Failure of energy stability in Oldroyd-B fluids at arbitrarily low Reynolds numbers," J. Non-Newtonian Fluid Mech. **135**, 92 (2006).
[29]M. Renardy, "Stress modes in linear stability of viscoelastic flows," J. Non-Newtonian Fluid Mech. **159**, 137 (2009).
[30]V. Gorodtsov and A. Leonov, "On a linear instability of plane parallel Couette flow of viscoelastic fluids," J. Appl. Math. Mech. **31**, 310 (1967).
[31]V. A. Romanov, "Stability of plane-parallel Couette flow," Funct. Anal. Appl. **7**, 137 (1973).
[32]M. Renardy and Y. Renardy, "Linear stability of plane Couette flow of an upper convected Maxwell fluid," J. Non-Newtonian Fluid Mech. **22**, 23 (1986).
[33]H. J. Wilson, M. Renardy, and Y. Renardy, "Structure of the spectrum in zero Reynolds number shear flow of the UCM and Oldroyd-B liquids," J. Non-Newtonian Fluid Mech. **80**, 251 (1999).
[34]A. S. Kumar and V. Shankar, "Instability of high-frequency modes in viscoelastic plane Couette flow past a deformable wall at low and finite Reynolds number," J. Non-Newtonian Fluid Mech. **125**, 121 (2005).
[35]S. A. Orszag, "Accurate solution of the Orr–Sommerfeld equation," J. Fluid Mech. **50**, 689 (1971).
[36]T. C. Ho and M. M. Denn, "Stability of plane Poiseuille flow of a highly elastic liquid," J. Non-Newtonian Fluid Mech. **3**, 179 (1977).
[37]R. Sureshkumar and A. N. Beris, "Linear stability analysis of viscoelastic Poiseuille flow using a Arnoldi-based orthogonalization algorithm," J. Non-Newtonian Fluid Mech. **56**, 151 (1995).
[38]D. G. Thomas, R. Sureshkumar, and B. Khomami, "Pattern formation in Taylor–Couette flow of dilute polymer solutions: Dynamical simulations and mechanism," Phys. Rev. Lett. **97**, 054501 (2006).
[39]D. G. Thomas, B. Khomami, and R. Sureshkumar, "Nonlinear dynamics of viscoelastic Taylor–Couette flow: Effect of elasticity on pattern selection, molecular conformation and drag," J. Fluid Mech. **620**, 353 (2009).
[40]K. Kim, R. J. Adrian, S. Balachandar, and R. Sureshkumar, "Dynamics of hairpin vortices and polymer-induced turbulent drag reduction," Phys. Rev. Lett. **100**, 134504 (2008).
[41]N. Hoda, M. R. Jovanović, and S. Kumar, "Energy amplification in channel flows of viscoelastic fluids," J. Fluid Mech. **601**, 407 (2008).
[42]N. Hoda, M. R. Jovanović, and S. Kumar, "Frequency responses of streamwise-constant perturbations in channel flows of Oldroyd-B fluids," J. Fluid Mech. **625**, 411 (2009).
[43]R. B. Bird, C. F. Curtiss, R. C. Armstrong, and O. Hassager, *Dynamics of Polymeric Liquids* (Wiley, New York, 1987).
[44]R. F. Curtain and H. J. Zwart, *An Introduction to Infinite-Dimensional Linear System Theory* (Springer, New York, 1995).
[45]J. A. C. Weideman and S. C. Reddy, "A MATLAB differentiation matrix suite," ACM Trans. Math. Softw. **26**, 465 (2000).
[46]J. Fontane, P. Brancher, and D. Fabre, "Stochastic forcing of the Lamb–Oseen vortex," J. Fluid Mech. **613**, 233 (2008).
[47]A. W. El-Kareh and L. G. Leal, "Existence of solutions for all Deborah numbers for a non-Newtonian model modified to include diffusion," J. Non-Newtonian Fluid Mech. **33**, 257 (1989).
[48]A. V. Bhave, R. C. Armstrong, and R. A. Brown, "Kinetic theory and rheology of dilute, nonhomogeneous polymer solutions," J. Chem. Phys. **95**, 2988 (1991).
[49]R. Sureshkumar and A. N. Beris, "Effect of artificial stress diffusivity on the stability of numerical calculations and the flow dynamics of time-dependent viscoelastic flows," J. Non-Newtonian Fluid Mech. **60**, 53 (1995).
[50]B. Thomases and M. Shelley, "Emergence of singular structures in Oldroyd-B fluids," Phys. Fluids **19**, 103103 (2007).
[51]This is an immediate consequence of the continuity equation and Eq. (C1); for fluctuations with $k_x=k_z=0$, the wall-normal velocity is identically equal to zero, while u and w, respectively, depend on τ_{12} and τ_{23}. Thus, the presence of initial conditions in τ_{22} yields zero initial kinetic energy.